sustainability

MDPI

Article

Synthesis, Characterization and Sorption Properties of Biochar, Chitosan and ZnO-Based Binary Composites towards a Cationic Dye

Hridoy Roy [1], Md. Shahinoor Islam [1,*], Mohammad Tanvir Arifin [1] and Shakhawat H. Firoz [2]

[1] Department of Chemical Engineering, Bangladesh University of Engineering and Technology, Dhaka 1000, Bangladesh
[2] Department of Chemistry, Bangladesh University of Engineering and Technology, Dhaka 1000, Bangladesh
* Correspondence: shahinoorislam@che.buet.ac.bd; Tel.: +880-29665650-80

Highlights:

The work analyzes the impact of chitosan and ZnO modification on surface and sorption characteristics of *Moringa oleifera* biochar. Moreover, statistical analysis was used to validate the experimental data.

What are the main findings?

- Chitosan modification enhanced the surface functional groups of raw *M. oleifera* biochar.
- The highest and lowest BET surface areas were found for BZ and BC, respectively.
- Chitosan-modified biochar showed a 75% increment in % removal of methylene blue compared to raw biochar.
- ZnO modification decreased the performance of biochar by 16%.
- Kinetics and Isotherm analysis of Chitosan-modified biochar align with statistical analysis.
- The adequate precision ratio was 52.80 and lack of fit *p*-value was 0.0018.

Abstract: Industrial effluents contaminated with different types of organic dyes have become a major concern to environmentalists due to the carcinogenic nature of the dyes, which are harmful to human and aquatic life. In recent years, the treatment of contaminated effluents by natural resources has been proposed as the most sustainable solution for this problem. In this work, *Moringa oleifera (M. oleifera)* seed-derived biochar composites, e.g., Biochar-Chitosan (BC), Biochar-ZnO (BZ), and Chitosan-ZnO (CZ) were produced and characterized. The synthesized materials were then utilized to adsorb a cationic dye, methylene blue. Spectroscopic analysis of the biochar-based composites revealed that the modification of biochar by chitosan and ZnO introduced different functional and active groups in the biochar surface. Pore development in the structure of biochar nanocomposites was visible in surface morphological images. The derived biochar was fully amorphous and increased crystallinity by the ZnO modification. The obtained surface area varied from 0.90 ± 0.00 to 14.48 ± 1.13 m^2 g^{-1} for prepared sorbents, where BZ corresponds to the highest and BC corresponds to the lowest surface area, respectively. The basic pH (9) was the most favorable condition for sorption. The sorption reached equilibrium at 90 min. Isotherm revealed the favorability of the Langmuir model over the Freundlich and Temkin models. The highest sorption capacity (~170 mg/g) was found for BC. The BC and BZ showed a 75% increase and 16% decrease in removal due to the chitosan and ZnO modification, respectively. Response surface methodology (RSM) optimization for BC showed similar results to the analytical experiments. The characterization and experimental results prefigure the chemical functionalities as the critical parameter over the surface area for the adsorption process.

Keywords: *M. oleifera* seeds biochar; binary nanocomposites; chemical functionalization; surface area; adsorption; RSM analysis

check for updates

Citation: Roy, H.; Islam, M.S.; Arifin, M.T.; Firoz, S.H. Synthesis, Characterization and Sorption Properties of Biochar, Chitosan and ZnO-Based Binary Composites towards a Cationic Dye. *Sustainability* **2022**, *14*, 14571. https://doi.org/10.3390/su142114571

Academic Editor: Changhyun Roh

Received: 7 September 2022
Accepted: 2 November 2022
Published: 5 November 2022

Publisher's Note: MDPI stays neutral with regard to jurisdictional claims in published maps and institutional affiliations.

Copyright: © 2022 by the authors. Licensee MDPI, Basel, Switzerland. This article is an open access article distributed under the terms and conditions of the Creative Commons Attribution (CC BY) license (https://creativecommons.org/licenses/by/4.0/).

1. Introduction

In the last few decades, modernization of the socio-economic structure of the world and the growth of different industries, e.g., fertilizer, textile, plastic, pharmaceuticals, pulp and paper, cosmetics, food, etc., the use of chemicals has accelerated at a concerning rate [1,2]. The uncontrolled discharge of the liquid effluents from these industries into the natural water bodies is a great concern to researchers and policymakers [3]. The azo dyes are extensively used chemicals in many industries, especially textile, paper and food industries, and need to be properly treated before discharging due to their toxic and carcinogenic nature [4,5]. Several techniques for treating dye wastewater have been developed and implemented, including advanced oxidation process (AOPs) [6–10], filtration [11], coagulation-flocculation [12], electrocoatgulation [8,10,13], ion exchange [14,15], biological treatment [16–18], photocatalysis [19–25], electrochemical treatment [26,27], and adsorption [28–35]. However, some of these methods are not applicable considering economic and environmental perspectives [31]. In some processes, an undesirable quantity of waste or residue is generated, which makes the process complicated and time-consuming [36]. Photocatalytic dye degradation is very efficient; however, it has several disadvantages, e.g., high cost and materials unavailability [23]. Among these treatment methods, the adsorption process has become very popular. Some advantageous features of the adsorption process, e.g., availability of diverse types of adsorbents, low production cost, energy efficiency, and ease of operation, have made it more feasible over the other methods [36,37]. In addition, the recyclability of the adsorbents allows the usage over several cycles, which makes it one of the most sustainable processes for dye wastewater treatment [38,39]. By adsorption, a bulk volume of industrial wastewater can be treated with no harmful residue [40,41]. In recent years, different adsorbents have already been reported e.g., silica gel [42], alumina [43], zeolites [44], bentonite clays [45], graphene oxide (GO) [46,47], activated-carbon (AC) [48,49], biochar [50–53], etc. However, silica gel, alumina, zeolites, GO, and bentonites are reported to be very efficient for removing dye from liquid phase, but the initial cost, unavailability of raw materials and complicated synthesis process are some major drawbacks that hinder the huge acceptability and applicability of these adsorbents in the large-scale water treatment process [54–56]. For large-scale operation, AC and biochar are found to be very efficient, in which AC preparation requires some sequential steps, e.g., carbonization and physical and chemical activations [29], whereas biochar preparation is very simple and facile [57–60]. In recent years, biochar has been extensively used for the sequestration of different types of organic dyes due to its large surface area, which provides adsorption sites for dye molecules; and, most importantly, different active functional groups of biochar surface that show attractive forces towards dye molecules [28]. The surface functional groups, e.g., carboxylic (-COOH), hydroxyl (-OH), amine (-NH_2), phenolic (Ph-OH), ether (R-O-R), etc., interact with the organic pollutants by electrophilic interaction along with physisorption [61], thereby separating dye from the aqueous media. The adsorbing properties of the biochar are directly affected by its parent source [62]. An appropriate biomass source that is readily available is a critical requirement for selecting an adequate parent source for biochar production [32]. The sorption capacities and interaction mechanisms of biochar with dye molecules rely on the ionic form (type and charge) of the dye, the chemical composition of biochar, the surface modification/activation process, the aging process, and environmental conditions [33]. Different bio-sources, e.g., sawdust, canola straw, rice straw, rice husk, citrus peel, peanut shell, pine wood, etc., are used to produce biochar [63]. However, the pristine biochar hardly exhibits high adsorption efficiency for capturing toxic organic pollutants and suffers from a lack of selectivity [64]. To overcome these constraints, emphasis has further been focused on the modification of biochar by different polymers, e.g., cellulose, pectin, chitosan and metal oxides e.g., CaO, CuO, ZnO [65]. Biochar modification enhances its surface functionality and pore structures [35]. The natural polymer (polysaccharides) modified of biochar has found to be very efficient due to the easy synthesis process, nontoxic residues, and improved sorption activity. Among the natural polysaccharides, chitosan serves the advantages of enhanced functional groups

and stability [66–68]. Moreover, the incorporation of amphoteric oxide such as ZnO in biochar has been found to be very efficient for the synergistic and nucleation effects of ZnO to increase the surface area and activities of biochar [69,70]. Moreover, the defects in ZnO structure also contribute to the dye sequestration (mainly by dye degradation not adsorption). However, the literature available for these modified materials are not comprehensive and deal with miscellaneous applications. Thus, this study considered an approach to investigate the ZnO and chitosan modification comparison on *M. oleifera* biochar's surface and sorption characteristics. The work has correlated different literature and utilized them for a comprehensive study on surface and sorption characteristics of ZnO and chitosan modified biochar.

Therefore, the main objective of the current study was to synthesize three different binary composites: i.e., biochar-chitosan (BC), biochar-ZnO (BZ) and chitosan-ZnO (CZ), and to investigate the performance of the binary composites in the adsorption of methylene blue (MB) cationic dye. Literature suggests the surface of biochar has abundant functional groups (negative); thus, a cationic dye MB was our choice for the experiment, as it would show the affinity towards the negative surface of the biochar and would be selectively adsorbed. Moreover, MB is a toxic azo dye that has extensive industrial use. Thus, industrial effluents are often characterized by a high concentration of these (azo) dyes. The specific objectives under the main objective were: (i) preparation of biochar from *M. oleifera* seeds feedstock, (ii) synthesis of BC, BZ and CZ from biochar with chitosan and ZnO, (iii) characterization of biochar for investigating the surface area, surface morphology and surface functional groups, (iv) investigation of adsorption behavior (using isotherm and kinetic study) for both pristine biochar, and binary composites against a cationic dye (MB), (v) analytical optimization of equilibrium conditions (optimum pH, contact time, and initial concentrations) to maximize the sorption, (vi) statistical optimization of adsorption using response surface methodology (RSM).

2. Materials and Methods

2.1. Materials

The *M. oleifera* seeds were collected from locally available vendors. The vendor also supplied the chemicals of analytical grade (used as received) obtained from Sigma-Aldrich (Germany) and Merck (Germany). The chemicals used in this work are listed as,

i pure chitosan ($C_{56}H_{103}N_9O_{39}$)
ii zinc oxide (ZnO)
iii ethanol (C_2H_5OH)
iv sodium hydroxide (NaOH)
v acetic acid (CH_3COOH)
vi nitric acid (HNO_3)
vii zinc nitrate (Zn $(NO_3)_2$)
viii methylene blue (MB)
ix deionized (DI) water

The regular lab accessories, e.g., conical flask, pipette, volumetric flask, cuvette, rotating shaker, sealed tube, spatula etc., were used as available in the laboratories.

2.2. Methods

2.2.1. Biochar (B) Preparation

The biochar was produced following one of our previous studies [34]. Briefly, the *M. oleifera* seeds were collected from the local market. The seeds were then dried and washed with pure ethanol to wash the inorganic impurities. The washed seeds were then dried in an air oven at 50 °C for 12 h. to keep the moisture content below 10%. The seeds were then crushed using a mechanical grinder, and 20 g of ground mass was fed into a muffle furnace under N_2 purge (N_2 purge flow: 1.0 L/h to replace the air inside the chamber). The biochar was prepared with a continuous N_2 flow (0.6 L/h) at about 350 °C with a heating rate of 5.8 °C/min at 2 bar pressure for 3 h. The biochar sample was then collected and mixed

with 15% nitric acid (HNO_3) solution under stirring at 40 °C for 4 h for chemical activation of the biochar surface. The sample was then washed with DI water until neutralized, and finally, neutralized material was dried at 105 °C for 12 h.

2.2.2. Biochar-Chitosan (BC) Preparation

The chitosan-modified biochar was prepared following Sajid Mehmood et al. (2020) [71], and some changes have been incorporated according to the available resources. In order to prepare the BC composite, 1 g of chitosan (as received) was mixed in 180 mL acetic acid (2 wt.%), and 3 g of the prepared biochar was then put into the prepared mixture. The mixture was then shaken using a stirrer for 30 min to form a uniform suspension. Then the biochar-chitosan homogenous suspension was added dropwise into a 900 mL NaOH (1.2 wt.%) solution and kept in the solution for 12 h. The mixture was repeatedly washed with DI water (to washout unreacted NaOH), and after being washed approximately 20 times, the mixture was oven-dried for 24 h at 105 °C to achieve the BC composite.

2.2.3. Biochar-ZnO (BZ) Preparation

The ZnO-modified biochar composite (BZ) was prepared by impregnation of the biochar powder into Zn $(NO_3)_2$ aqueous solutions. Initially, biochar was pretreated using Zn $(NO_3)_2$ solution (the mass ratio was 1:1). After the addition of Zn $(NO_3)_2$, the adsorbent was dried at 105 °C for 12 h. Then the Zn $(NO_3)_2$-pretreated biochar was mixed with 0.1 M NaOH and pyrolyzed at 380 °C for 1 h. under an N_2 atmosphere to obtain BZ. Subsequently, the sample was naturally cooled to ambient temperature to obtain the final adsorbent [72].

2.2.4. Chitosan-ZnO (CZ) Preparation

Chitosan-ZnO composite was prepared following (with some modifications) Arafat Abul et al. (2015) [73]. To prepare the CZ composite, initially, a 2.0 g of ZnO powder was added into 1% acetic acid solution, followed by the addition of 1.0 g of chitosan to the CZ mixture. After vigorous magnetic stirring and sonication for 30 min, 0.10 N NaOH was added dropwise to reach the solution pH of 7, and then the solution was treated at 75–80 °C for 3 h. Then the solution was dried in an air oven at 50 °C for 1 h.

2.3. Characterization of Adsorbents

Different characterization techniques were used for *M. oleifera*-derived biochar and other binary composites to confirm the preparation and modification feasibility. Fourier transform infrared (FTIR) spectroscopy was performed using an FTIR-8400 instrument (Shimadzu, Japan). The spectra were taken from the 4000 to 400 cm^{-1} range. X-ray diffraction (XRD) was performed using a RIGAKU Ultima IV diffractometer (Rikagu corporation, Tokyo, Japan) in 2θ range from 10 to 80°. A field emission scanning electron microscope (FESEM) (JEOL Ltd., Tokyo, Japan) was used to collect SEM images to evaluate the surface morphological structure. A PulseChemiSorb 2705 was applied to measure surface area.

2.4. Isotherm and Kinetics Experiments

Adsorption characteristics of *M. oleifera* seed biochar, chitosan, ZnO, BC, BZ, and CZ, were systematically analyzed by varying the factors of sorption, e.g., solution pH, sorption time (t (min) and initial concentration of dye (Co (mg/L)). The sorbent dosage was kept at 0.2 g/L to carry out all isotherm and kinetic experiments, and the temperature for all the reactions was 29 ± 2 °C. The pH effect was investigated in the range of 3.0 to 11.0. The kinetic sorption experiments were carried out for 180 min to achieve the equilibrium time for 60 mg/L dye solution at 29 ± 2 °C. The samples were collected at different time intervals ranging from 15 to 180 min. The sorption isotherms experiments were conducted with seven different dye solutions (concentration range: 10–70 mg/L) for 90 min. For the pH test, we took 0.2 g/L of each sorbent for a specific pH and performed 6 (no. of adsorbents) × 5 (pH variation) × 2 (replication) = 60 experiments. The average of the 2 tests was taken. For kinetics and isotherms, we have executed experiments similarly. The precipitate containing

biochar/binary composites was separated, and the supernatant solution was filtered using a 0.45 µm nylon filter and analyzed for residual dye concentration using a SHIMADZU UV–Vis spectrophotometer-1601, Japan.

The % removal and sorption capacity of tested samples were evaluated using Equations (1) and (2), respectively [29].

$$\% \text{ Removal} = \frac{(C_o - C_e) \times 100}{C_O} \quad (1)$$

$$\text{Adsorption Capacity, } q\left(\frac{mg}{g}\right) = \frac{(C_o - C_e) \times V}{m} \quad (2)$$

C_o and C_e in Equations (1) and (2) indicate initial and residual dye concentrations (mg/L) at equilibrium, V is the dye volume taken in which m (g) of sorbents were used for each experiment, and q (g/mg) represents the mg of dye adsorbed onto per g of adsorbents.

2.5. Statistical Design

To validate the experimental data for further reliability, in this work, we have used Design Expert Software (version 6.0.11) for statistical analysis by applying the central composite design (CCD) model. The response surface methodology (RSM) was used to interpret the individual parameter such as time = X_1, the concentration of dye = X_2 and pH = X_3) effects on % removal The RSM was done only for BC. To avoid exaggerating (RSM on one sorbent can give enough information to check the viability of the experiments), only BC was selected to conduct statistical analysis as analytical experiments found the functionalization by chitosan was way more successful compared to others. The coded and uncoded levels of RSM design are summarized in Table 1.

Table 1. The individual parameters and their coded levels of BC composite for MB dye removal (%).

Parameters	Notation	Coded Levels				
		$-\alpha$	−1	0	+1	$+\alpha$
Time (min)	X_1	7.5	10	65	120	157.5
Concentration (mg/L)	X_2	9.5	10	35	60	77.0
pH	X_3	0.7	2	6	10	12.7

The CCD was used in our case, as this model provides more flexibility over others. Twenty (20) experimental runs were executed according to the statistical design. In the 20 experiments, six (6) axial points, eight (8) fractional factorial points and six (6) central points were randomly performed according to CCD for a better prediction of the sorbate-sorbent system. An in-depth understanding of the effect of operating variables on response variables was generated using 3D response plots by Design Expert Software (version 6.0.11). The range of variables was selected with the help of the results of prior analytical tests. The highest and lowest coded values for X_1, X_2 and X_3 were (10, 120), (10, 60) and (2, 10), respectively.

2.6. Isotherms and Kinetics Modeling

In order to validate the obtained data and understand the in-depth sorption process, three isotherm models, e.g., Langmuir, Freundlich and Temkin, were utilized.

The Langmuir model interprets the homogeneous sorption processes and implies that the surface of the sorbents has a limited number of active sites accessible to each dye molecule equally and allows uniform monolayer adsorption [28]. The linear form of the Langmuir model is:

$$\frac{C_e}{q_e} = \frac{1}{q_m k_L} + \frac{C_e}{q_m} \quad (3)$$

C_e in Equation (3) indicates equilibrium dye concentrations (mg/L), k_L (L/mg) is the Langmuir isotherm constant, q_e (g/mg) represents the mg of dye adsorbed onto per g of adsorbents at equilibrium for a specific dye concentration and q_m (mg/g) is the maximum mg of dye adsorbed onto per g of adsorbents.

The Freundlich isotherm model was developed on the basis of heterogeneous and multilayer sorption concepts [74]. The linear Freundlich model is:

$$\ln q_e = \ln k_F + \frac{1}{n} \ln C_e \quad (4)$$

Here, k_F (mg/g) is the Freundlich isotherm constant (mg/g), n is the constant depends on the nature of the adsorbate and adsorbent, 1/n (values between 0 to 1) indicates the favorability of the isotherm, qe and C_e has the same meaning as before.

The Temkin model is based on the concept of the indirect interaction of the sorbent and dye molecules [75]. The form of the Temkin model is as follows:

$$q_e = b_T \ln k_T + b_T \ln C_e \quad (5)$$

where b_T (kJ/mol) is the Temkin isotherm constant and k_T (L/g) is the Temkin isotherm equilibrium binding constant (L/g).

To know whether the sorption process is dominated by physisorption or chemisorption, the sorption kinetics were evaluated using the pseudo-1st order and pseudo-2nd order models.

The pseudo-1st order model assumes physisorption [76]. It is expressed as Equation (6),

$$\ln(q_e - q_t) = \ln\ q_e - k_1 t \quad (6)$$

Here, q_e (g/mg) and q_t (g/mg) represent the mg of dye adsorbed per g of adsorbents at equilibrium for a specific dye concentration, and q_t (mg/g) represents the mg of dye adsorbed per g of adsorbents at a time; and k_1 is the pseudo-1st order rate constant of adsorption (h^{-1}).

In the pseudo-2nd -order model, chemisorption is assumed to be the rate-limiting step [28]. It is expressed as Equation (7):

$$\frac{t}{q_t} = \frac{1}{k_2 q_e^2} + \frac{t}{q_e} \quad (7)$$

Here, k_2 is the pseudo-2nd order rate constant, and other symbols carry the same meaning as before.

3. Results and Discussions

3.1. Materials Characterizations

The FTIR spectra of prepared *M. oleifera* biochar, binary composites BC, BZ, and CZ, were presented in Figure 1A. The surface of biochar was decorated with different functional groups, which are evident in Figure 1A (black line). The bands at 2920–2860 cm^{-1} and 1630 cm^{-1} attributed to the aliphatic C–H bonds and C=O stretching of a carbonyl (C=O.) or carboxylic groups (-COOH), respectively. The symmetrical bending of methyl groups ($-CH_3$) was presented by the peak at 1385 cm^{-1}. The characteristic peak at 1103 cm^{-1} predicted the presence of C=O bonds of ester or phenolic groups [77–79].

The hydroxyl (-O–H) stretching vibration of surface-bound H_2O may give a wide peak at 3430 cm^{-1} [80,81]. The FTIR spectrum of the BZ composite (orange line) exhibited peaks at the lower wavenumber region, which is indicative of the ZnO addition [82]. The Zn-O stretching band at 900 and 539 cm^{-1} was observed [72]. Some of the peaks at BZ were reduced in intensity compared to biochar, which is suggestive of the bond formation of functional groups of biochar with ZnO. In the CZ composite (blue line of Figure 1A), the peak at 1383 cm^{-1} may attribute the stretching of the C-N bond for amide III [83] to the presence of

N-acetyl groups from chitosan. At 2930 and 2860 cm^{-1}, the peaks associated with the C–H stretching vibration; and the peaks available around 1167 cm^{-1} (C–O stretching vibration) and 450 cm^{-1} (Zn–O stretching) are also suggestive of the successful preparation of the binary composites [84].

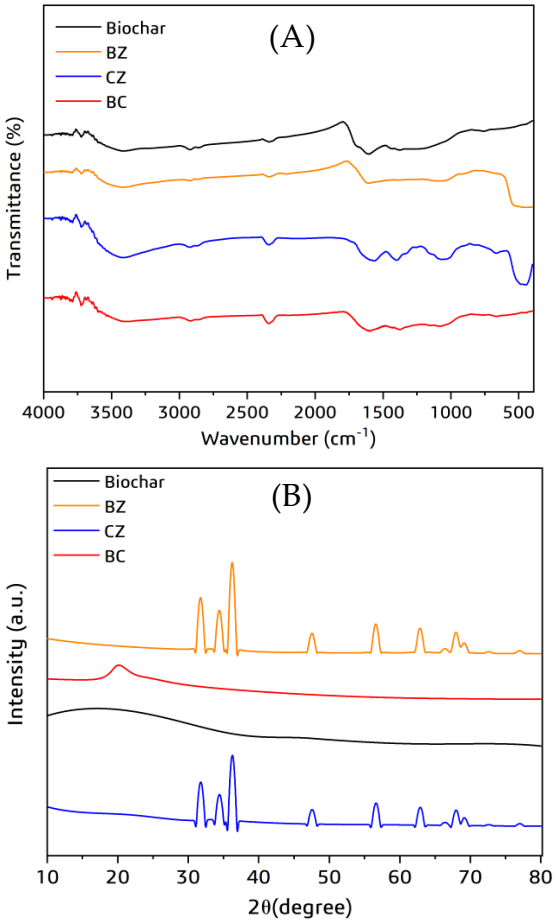


Figure 1. Comparison of the FTIR spectra (**A**) and XRD peaks (**B**) of biochar, BC, BZ, and CZ.

In the FTIR spectrum of BC, the band at 1084 cm^{-1} corresponds to the free amino group at C_2 of glucosamine [85]. A peak at 1375 cm^{-1} was observed, corresponding to the C=O stretching in the primary alcoholic group of chitosan. The OH stretching frequency at 3425 cm^{-1} was attributed to the free phenol groups. The primary amine (-N-H) bending and wagging at 1625 cm^{-1} and 890 cm^{-1} were observed, respectively. The peak near 2300 cm^{-1} may correspond to -NCO or -CN groups. This peak was intense in BC and CZ, compared to biochar. The presence of chitosan may provide the -N for these groups' formation. Natural ammines groups in biochar surfaces can also form these groups [86]. The surface of BC exhibited the characteristic peaks of biochar and chitosan, which make BC a highly functional composite. The abundant reactive functional entities of BC may contribute to the sorption process by the interaction with counterparts available in MB molecules.

The XRD patterns of biochar, BZ, CZ and BC were presented in Figure 1B. The *M. oleifera* biochar (black line) was amorphous with no sharp peaks. The decomposition of cellulosic materials may result in this amorphocity [87]. Therefore, biochar had an amorphous structure with randomly oriented aromatic carbon sheets [88]. The BC composite was amorphous with a single peak at 2θ~20 ° (red line), which may be associated with chitosan. The XRD pattern of the BZ composite (orange line) exhibited several peaks with two intense peaks at 2θ~31.7° and ~36.25° corresponding (1 0 0) and (1 0 1) planes, respectively. These planes confirmed the typical nonlinear 3D carbon with the disordered structure of

biochar. The sharp peaks of the CZ composite (blue line) correspond to the ZnO with a high crystallinity in structure.

Figure 2 presents the surface morphologies (FESEM image) of biochar and binary composites. In addition, the elemental composition of biochar and binary composites obtained from Energy -dispersive X-ray spectroscopy (EDS) was presented in Table 2.

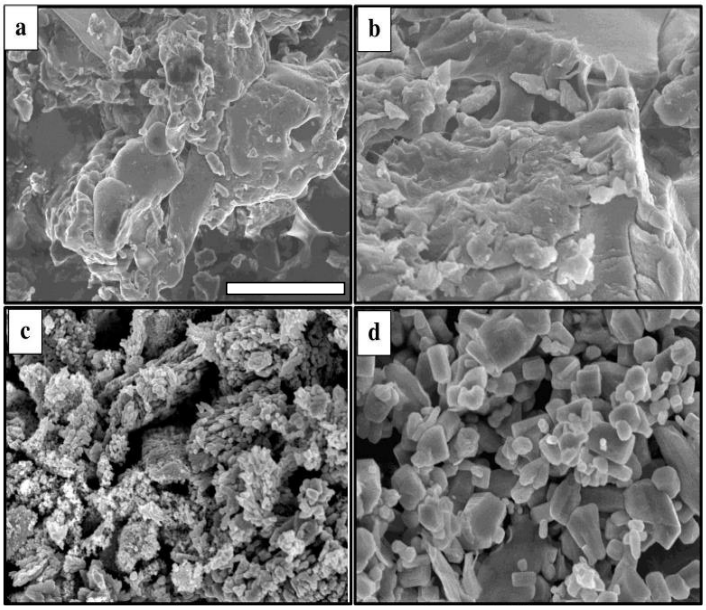


Figure 2. Scanning electron microscope (SEM) micrograph of biochar (**a**), BC (**b**), BZ (**c**), and CZ (**d**) (×20,000 magnification) and bar of 10 micrometers).

Table 2. Elemental composition of prepared samples from Energy -dispersive X-ray spectroscopy (EDS). BC, BZ represents Biochar-chitosan, Biochar-ZnO, and chitosan-ZnO.

Sorbents	Composition			
	Carbon (%)	Nitrogen (%)	Oxygen (%)	Zinc (%)
Biochar	70.12	17.10	12.13	-
BC	70.31	12.64	17.79	-
BZ	14.94	1.63	46.21	37.21
CZ	57.22	2.78	13.89	26.11

The presence of macropores and irregular troughs in the biochar surface is visible in Figure 2a [89]. The disintegration and volatilization of biochar feedstocks formed mixtures of different gaseous substances in the biochar structure [90]. The formation of cracks was due to the result of long residence time in the furnace [91], and the macropores were produced by combining adjacent micropores by gas escaping in the volatilization phase. The phenomenon of macropore formation decreased the surface area of biochar (evident in BET surface area results) [92]. From Figure 2b, the irregular-shaped BC particles were observed. The surface had some rough cracks, irregular blocks, some crystalline clusters, and disordered membrane fissures. The presence of significant pores and the specific existence of chitosan particles were not observed from the FESEM image. The higher O% in the BC compared to biochar was observed from the EDS results (Figure 2b and Table 2). It indicates the increased oxygenated functionalities of BC. The presence of C=O, -COOH and -OH groups increased O content in the BC surface, which is supported by the FTIR results [93]. The BZ particles resembled the coral-shaped random 3D structure (Figure 3c). The ZnO incorporation may create a tunnel-like crack in the surface. The spherical ZnO clusters were visible in the FESEM image. The crystalline ZnO particles provided the

pyrolysis nucleation center for forming more cracks around ZnO, which increased the specific surface area of the BZ composite [94]. The presence of C, O, Zn and trace N were found in the BZ sample. The wt% of C, O and Zn was found to be 14.94, 46.21 and 37.21, respectively (Table 2). The pore formation in the BZ composite is indicative of the reaction of NaOH and carbon, which formed CO_2. The resulting CO_2 may react again with NaOH resulting in the deposition of Na_2CO_3 forming a rough surface. The macropores, and visible channels may form due to the CO_2 diffusion through the internal structures of BZ [69]. The Zn modification provided the nucleation center. As a result, agglomeration occurs with the biochar surface [95].

$$4NaOH + 2CO_2 \leftrightarrow 2Na_2CO_3 + 2H_2O$$

$$4NaOH + C \leftrightarrow 4Na + CO_2 + 2H_2O$$

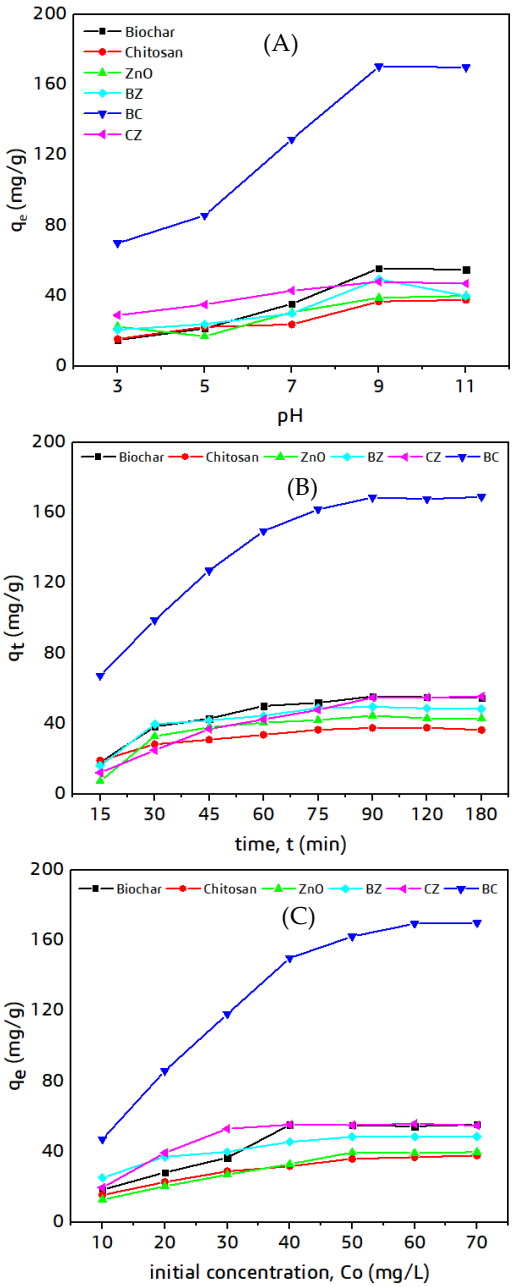


Figure 3. Effect of pH (**A**), time (**B**) and initial concentration (**C**) on adsorption of MB by biochar, chitosan, ZnO, BZ, CZ and BC.

The BET-specific surface area of prepared biochar and binary composites BC, BZ, and Z was summarized in Table 3.

Table 3. BET surface area of biochar, BC, BZ and CZ. BC, BZ represents Biochar-chitosan, Biochar-ZnO, and chitosan-ZnO.

Sorbents	Surface Area (m^2 g^{-1})
Biochar	0.96 ± 0.00
BC	0.90 ± 0.01
BZ	14.48 ± 1.03
CZ	1.99 ± 0.00

The ZnO-modified BZ showed the highest surface area of 14.48 ± 1.03 m^2 g^{-1}, whereas the chitosan-modified BC composited had the lowest surface area of 0.90 ± 0.01 m^2 g^{-1}. The FESEM images (Figure 2) were also suggestive of the obtained BET surface area, as BZ had a more porous and rougher surface compared to BC. The chitosan modification has decreased the surface area of biochar to a small extent, suggestive of the pore blockage of biochar. However, the ZnO incorporation significantly increased the surface area due to the nucleation of ZnO onto the biochar surface, introducing several pores in the BZ structure.

3.2. Effect of pH on Sorption

The initial pH of the dye solution is an important and controlling parameter for the sorption process [96]. The sorption capacities of the sorbents with varying pH (3–11 range) were illustrated in Figure 3A.

The increasing pH induced the sorption capacities of the sorbents. This is due to the competitive effect of H^+ and MB molecules. The MB molecules are a cationic entity (at acidic pH, abundant H^+ ions restrict reaching MB molecules to the sorbents surface, which decreases the adsorption of MB dye molecules on the surface [97]. However, the uptake of MB was highly triggered by the increase in solution pH. The deprotonation of the oxygenated functional groups in the sorbent surface created a lot of negative charges that attracted the positive MB molecules [98]. This effect was more significant for the BC composite. At higher pH, the available carboxylic and alcoholic groups of BC possibly created –COO^- and–OH groups that contributed to the sorption of MB. Moreover, at higher pH, the abundant OH^- ions might increase the surface negativity of chitosan by blocking -NH_2, which further increases the sorption of MB molecules [99]. In Figure 3A, a slight decrease in sorption capacity was observed at pH > 9 due to the possible presence of excessive OH- ions that limited the available surface of sorbents. Amode et al. (2021) also reported the phenomenon of decreased sorption of MB in a highly alkaline medium by waste-based adsorbent [100]. From the correlation of pH with sorption capacity, electrostatic interaction (−ve surface functional groups and +ve MB molecule) was suggestive of being the primary mechanism of adsorption of MB dye onto BC at higher pH [40]. The lower surface area of BC exhibited higher sorption, which is indicative that the MB sorption onto BC may not be limited to surface sorption and pore diffusion only. Some other mechanisms, e.g., hydrogen bonding and π-π interaction, may also contribute to the sorption process [101].

3.3. Effect of Contact Time and Kinetics

Figure 3B shows the effect of contact time on sorption in the range of 15–180 min at 25 °C for biochar, chitosan, ZnO, BC, BZ and CZ, and the sorption capacities were 55, 47, 50, 170, 51, and 52 mg/g, respectively. The dye molecules were adsorbed to the sorbent surface quickly in the first 30 min. After that, the rate of sorption was slowed down gradually, and after 90 min, the rate was at a steady state. At first, the sorption rate for dyes was very high due to the abundance of accessible adsorption sites. Dye aggregation at the surface slowed adsorption as the available sites became increasingly occupied. It was assumed

that the improved performance of BC corresponded to the surface functional groups [102]. The primary amine groups and carboxylic groups (at alkaline pH) of chitosan and -COOH, -OH, ester, and phenolic groups of biochar are thought to bind MB molecules [103]. However, the equilibrium time was not exactly the same for all the sorbents. The saturation time may be impacted by the number of active sites available for each material, which is subjected to the available porosity, cracks, and functionality of the structure.

The MB sorption kinetics onto biochar, chitosan, ZnO, BC, BZ, and CZ were studied from 0 to 120 min timespan for a dye concentration of 60 mg/L with 0.2 g/L adsorbent dosages). For kinetic studies, pseudo-1st and pseudo-2nd were used [31]. At the initial stage of sorption, the free active sites of the sorbents promote the rapid capturing of MB molecules (Figure 3B) [104]; these sites become saturated with time [105], which leads to decreasing sorption of MB molecules [106].

Figure 4A,B and Table 4 illustrate and summarize the model fitting factors for biochar, chitosan, ZnO, BC, BZ, and CZ. The pseudo-2nd-order model better fits the kinetic data (R^2 ranging from 0.94 to 0.99) than the pseudo-1st-order (R^2 ranging from 0.70 to 0.92) for all the sorbents. The highest experimental sorption capacity ($q_{e,\,exp}$) was closer to the calculated sorption capacity ($q_{e,\,calc}$) from the pseudo-2nd model and suggestive of the adsorption being a chemisorption-dominated process. For BC, the q_e (175.40 mg/g) obtained from the pseudo-2nd order was close to the experimental value of 177 mg/g. The interaction of MB molecules with functional groups, e.g., deprotonated carboxylic, hydroxyls, esters, phenols, and diffusion of MB through micro and macro-pores, may contribute to the adsorption process [107].

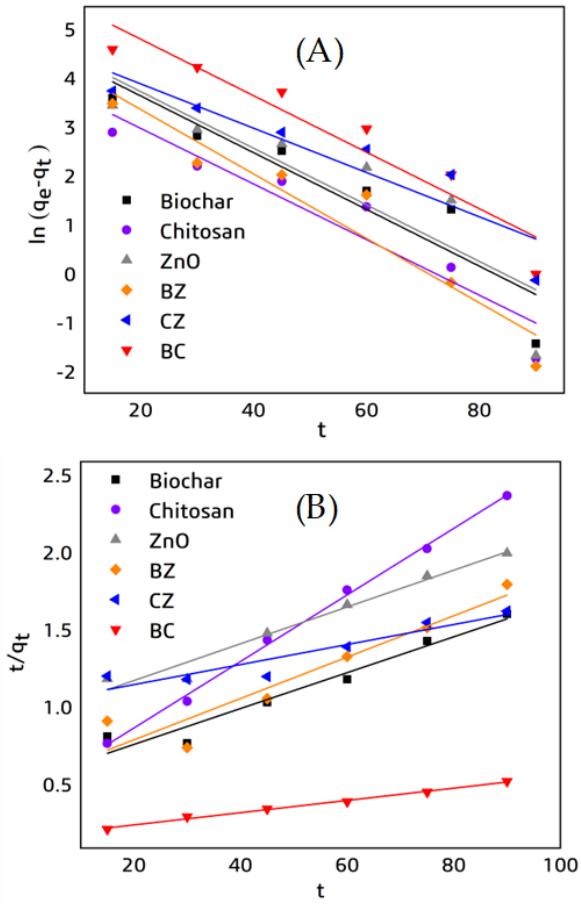


Figure 4. Linear fittings of pseudo-first (**A**) and pseudo-second (**B**) order kinetics for biochar, chitosan, ZnO, BC, BZ and CZ.

Table 4. Kinetics modeling parameters obtained for pseudo-1st order and pseudo-2nd order models.

Adsorbents	q_e Exp (mg/g)	Pseudo-1st Order			Pseudo-2nd Order		
		R^2	q_e Calc (mg/g)	k_1 (min^{-1})	R^2	q_e Calc (mg/g)	k_2 ($g \cdot mg^{-1} min^{-1}$)
Biochar	55.70	0.82	49.40	0.058	0.95	60.60	4.95×10^{-4}
Chitosan	38.15	0.88	24.60	0.056	0.99	41.67	1.30×10^{-3}
ZnO	40.10	0.71	51.95	0.057	0.96	43.47	5.57×10^{-4}
BC	162.15	0.85	134.30	0.059	0.99	175.40	1.91×10^{-4}
BZ	48.90	0.92	33.10	0.070	0.94	52.63	6.68×10^{-4}
CZ	55.15	0.80	36.60	0.045	0.94	58.82	2.83×10^{-4}

The k_1, k_2, and R^2 values in (Table 4) state the prime contribution of the functional groups of BC in the sorption process [108]. This means that the chemisorption process dominates over physisorption [109], and functionalities of both biochar and chitosan combine to give enhanced sorption to MB dye. The oxygen-containing functional groups of biochar and carboxylic/ammines of chitosan boosted the increased sorption capacity of BC [109], which might lead to the chemisorption of dye on the sorbent surface, indicating a pseudo-2nd order model of adsorption. However, the contribution of the surface structure of BC may not be the limiting factor for the sorption process. The enhanced surface area BZ resulted in poor sorption capacity, which established the fact that surface diffusion was not controlling the process. The surface chemistry that leads to the improved surface area, still low sorption capacities have to be revealed in the future, which would require some additional experimental and characterization verifications.

3.4. Effect of Initial Concentration and Isotherms

Figure 3C depicts the impact of initial dye concentrations (C_o) on sorption in the range of 10–70 mg/L. The sorption capacity increased as the initial dye concentration was raised from 10 to 70 mg/L for all the sorbents. When the concentration of the solution is raised, it exerts a strong force on the MB molecules, which leads to high sorption of MB [110]. In the first stage of adsorption, the surface functional groups were available to capture [111]; however, saturation was reached at ~50 mg/L for the sorbents [112]. The equilibrium sorption on BC (177 mg/g) is much higher than other sorbents, which further indicates that the chitosan modification of biochar enhances the activity of biochar due to the introduction of active sites and synergistic effects [113].

Isotherm modeling serves as the basic tool to study a sorption process [114]. Several isotherm models of biochar-based composites have been proposed to describe the liquid phase adsorption of contaminants [115]. Among these proposed models, Langmuir, Freundlich and Temkin models are well-recognized and widely applied isotherm models for organic adsorption in a solid-liquid system [116].

The Langmuir isotherm model describes sorption as monolayer coverage of the active sites of the sorbent, which are distributed in a homogenous energy perspective [29]. The Freundlich isotherm describes sorbent/sorbate system multilayer sorption heterogeneous surfaces [117]. The Temkin model predicts the sorption heat decrease linearly with active site blockage by foreign molecules.

The isotherm of biochar, chitosan, ZnO, BC, BZ and CZ systems using linear Langmuir, Freundlich and Temkin models was analyzed. The parameters of the models and representation of the linear fittings are summarized and presented in Table 5 and Figure 5A–C, respectively.

Table 5. Isotherm modeling parameters obtained for Langmuir, Freundlich, and Temkin Isotherms.

	R^2	k_L (Lmg^{-1})	q_m (mg/g)	R^2	k_F (mg/g). $(Lmg^{-1})^{1/n}$	1/n	R^2	b (kJ/mol)	k_T (dm^3/g)
Biochar	0.96	0.048	78.92	0.83	7.27	0.533	0.84	132.56	0.40
Chitosan	0.99	0.066	47.73	0.87	7.36	0.413	0.90	233.45	0.61
ZnO	0.98	0.036	60.27	0.86	4.41	0.561	0.91	177.41	0.31
BC	0.99	0.396	179.85	0.85	13.66	0.648	0.90	38.68	0.26
BZ	0.99	0.169	54.22	0.90	17.87	0.262	0.89	258.35	3.23

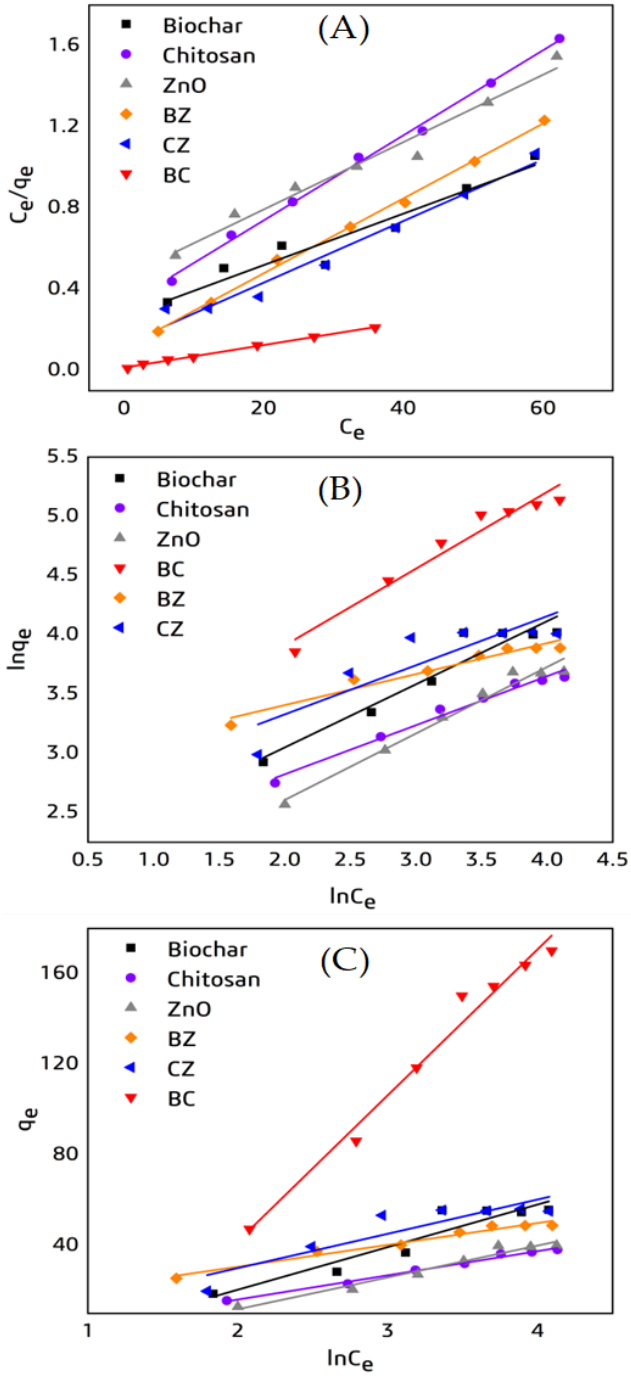


Figure 5. Linear fittings of Langmuir (**A**), Freundlich (**B**), and Temkin (**C**) isotherm for biochar, chitosan, ZnO, BC, BZ, and CZ.

The R^2 value of the Langmuir model varied from 0.96 to 0.99, the Freundlich model yielded the R^2 ranging from 0.83 to 0.90, and the R^2 from the Temkin model was between 0.83 to 0.91, indicating the fitting of the Langmuir model with the sorbents-MB system was more precise than the Freundlich and Temkin models, that indicates monolayer coverage of surface active sites by MB dominated over other mechanisms [118]. The Langmuir model gave the maximum sorption capacities of ~78, 55 and 180 mg/g for biochar, BZ and BC, respectively. The surface functional groups of biochar and chitosan may contribute in this case, where the enhanced surface area of BZ may trigger inter-pore diffusion, which resulted in low sorption compared to others [106].

However, it is not possible to cancel out the chances of the sorption of MB by multilayer sorption with heterogeneity, as the R^2 obtained from the Freundlich model was also in a good range. The electrostatic attach action between -NH_2 (chitosan), and oxygenated functional groups (biochar) may lead to the capture of MB [119,120]. The H-bonding of the oxygenated groups of biochar and less electronegative atoms fo dye molecules may also contribute to this phenomenon [59,121,122].

3.5. Response Surface Analysis for BC

3.5.1. The Model Fitting

To support the experimental result, response surface methodology (RSM) was utilized. Table S1 (Supplementary materials) presents the results of twenty experimental runs at different combination of X_1, X_2 and X_3.

The individual parameter has affected the % removal of BC. The analysis of variance (ANOVA) revealed that the fit of quadratic model (coefficient of determination, R^2 = 0.99) with experimental data was much better compared to linear model (R^2 = 0.61), and 2FI (R^2 = 0.58) model [123]. The $R^2_{\text{quadratic model}}$ was close to unity. Regression equation from RSM is expressed in Equation (8). The experimental data were used to evaluate the values of the coefficients in Equation (8) were computed from obtained experimental data.

$$\begin{aligned}(\%)\text{Removal} = \; & 6.58596 + 0.128066 * X_1 + 0.0507444 * X_2 + 17.1578 \\ & * X_3 + 5.45455e - 05 * X_1 * X_2 + 0.0197935 * X_1 * X_3 \\ & + - 0.009 * X_2 * X_3 + -0.000902599 * X_1^2 \\ & + - 0.00530844 * X_2^2 + -1.02372 * X_3^2\end{aligned} \quad (8)$$

The impact levels of each coefficient of the derived models were calculated by applying ANOVA, and the computed values are reported in Table S2 (Supplementary Materials).

The F-value of the obtained model was 249.38, with a very low *p*-value of <0.0001. This lower *p*-value justifies that, in this BC/dye system, there is only a 0.01% chance of creating noise to obtain an F-value [124]. In our case, considering high sensitivity, *p*-values less than 0.05 indicate model terms to be significant. In the BC/dye system, A, B, C, and C^2 were significant model terms. An adequate precision ratio of greater than 4 is acceptable, in our case, it was 52.80 (excellent signal-to-ratio). The lack of fit value for Equation (8) was found to be 37.32, which validates the statistical justification of the developed model for BC due to the non-significant lack of fit. The reasonable predictability of the system by the RSM model was also justified. In our model, there was only 1.80% of a significant lack-of-fit F-value could occur due to noise in the experiment (lack of fit *p*-value was 0.0018 (α)) [125]. The BC/MB system was found statistically stable.

3.5.2. Impact of Independent Variables on Response Variable

The RSM obtained 3D surface graphs were utilized to analyze the MB bye sorption phenomenon by BC. The 3D plots of (i) pH, time, (ii) pH, concentration and (iii) time, concentration was obtained by varying these parameters (time, pH and concentration) within the experimental ranges (Table 1). The correlative representation of different parameters affecting the removal efficiency of BC is shown in Figure 6A–C.

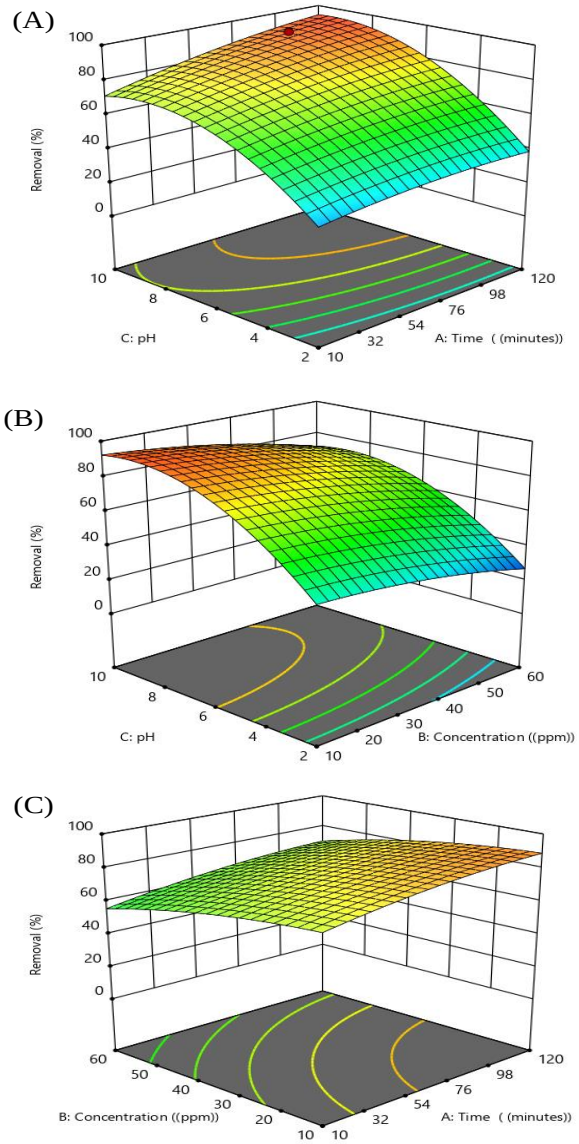


Figure 6. Combined effects of (**A**) pH and time, (**B**) pH and concentration and (**C**) concentration and time on removal (%) for BC.

Figure 6A presents increasing pH and contact time increased removal efficiency. At lower pH, the BC surface had abundantly available protons (H^+) in the sorbent-sorbate system, which enhanced the repulsion of MB dye onto the BC surface [126]. However, at higher pH (pH > 7), BC surface negativity will be increased, which attracts the MB molecules. With increasing time, removal reached equilibrium due to the saturation of the active sites of BC over time. Figure 6B illustrates that basic pH and low concentration gives high removal. In Figure 6C, at a constant pH, lower removal was achieved with higher dye concentration. The increase in time increases the removal, which supports the analytical results. Figure 6C presents the quadratic relation of MB concentration and time on removal efficiency. At higher concentrations, the removal of MB dye was decreased due to the surface exhaustion of BC. After reaching equilibrium, further increments in time caused zero impact on the adsorption of dye due to the surface saturation of the BC by MB dye [127].

4. Comparative % Removal of the Sorbents, Proposed Adsorption Mechanism for BC

The % removal of the sorbents is an important parameter to conclude the efficiency of a sorbent in a sorbate-sorbent system [31]. The comparative % removal of different sorbents

was presented in Figure 7 for pH of 9, dye concentration of 60 mg/L and contact time of 120 min.

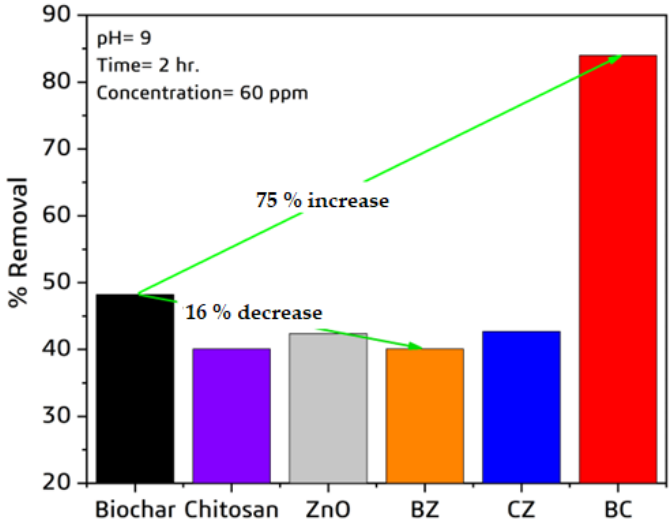


Figure 7. Comparative % removal of biochar, chitosan, ZnO, BZ, CZ and BC.

The biochar, chitosan, ZnO, BZ, CZ and BC showed a % removal of 47.5, 40, 43, 41, 44 and 83.5%, respectively. The obtained % removal for BC from the statistical analysis was 85.1%, which is very close to the analytically obtained results at the same optimized conditions.

The chitosan modification introduced a 75% increase in sorption capacity compared to raw biochar, whereas the ZnO incorporation reduced the sorption capacity by 16%. Thus, the chitosan modification was highly successful in our case. However, it is not indicative that ZnO modification always lowers the efficiency of biochar. The efficiency of the modification depends on the utilization of the composite. Therefore, chitosan-modified biochar can be an emerging material for sorptive water treatment, whereas ZnO modification may not be a good approach for sorption systems.

A probable MB sorption route by BC was proposed in this portion. A sorption process is validated by a combination of different mechanisms depending on the sorbent-sorbent system's characteristics and interactions. There are different types of available mechanisms, e.g., pore diffusion, electrostatic interaction, hydrogen bonding, and π-π interaction, to explain a specific system [122]. In our case, the lowest active surface area was achieved in BC. However, it has shown the highest sorption. Therefore, the surface area may not have the greatest contribution to MB sorption by BC in this case. The important removal mechanisms probably were electrostatic interactions, hydrogen bonding (H-bond), and π-π interaction of surface functional groups of BC with the dye molecules [33]. The proposed sorption mechanism for the MB dye onto BC is presented in Figure 8.

The small surface area of BC may not facilitate porous diffusion. The external diffusion of the MB molecules from the boundary layer to the BC surface may cause some of the MB molecules to be captured [128]. At basic pH, the electrostatic attraction between the functional groups of BC and MB molecules may play a significant role. FTIR reveals the presence of different functional groups, e.g., -OH, -COOH, R-COOH, R-OH, -NH_2, and aromatic structures (phenol, quinones, etc.) on the surface of the BC. At basic pH, the functional groups may deprotonate and attract the MB molecules [129]. The H-bonding interaction may occur between the functional groups on the BC surface and the nitrogen in dyes (i.e., nitrogen atoms in the MB molecules, which act as the H-acceptors) [130]. The π-acceptor and π-donor interaction may also play an important role in this case. The aromatic rings in the graphitic layer of BC (evident from XRD) may act as π-electron donors, and the aromatic rings in MB dye act as π-electron acceptors [131]. Also, molecular structures of MB possess a cation N^+, which may lead to the binding of cation N+ to the π-face of aromatic rings in the adsorbent surface, forming π+-π interaction. Therefore, the combination of

these mechanisms may provide BC with a strong adhesion toward MB [33]. Thus, based on the results and discussions above, the relative contribution of these mechanisms in the sorption of MB may be the following, (i) electrostatic interaction (strong influence), (ii) H-bonding (moderate), (iii) π-π interaction (moderate), (iv) pore diffusion (low influence).

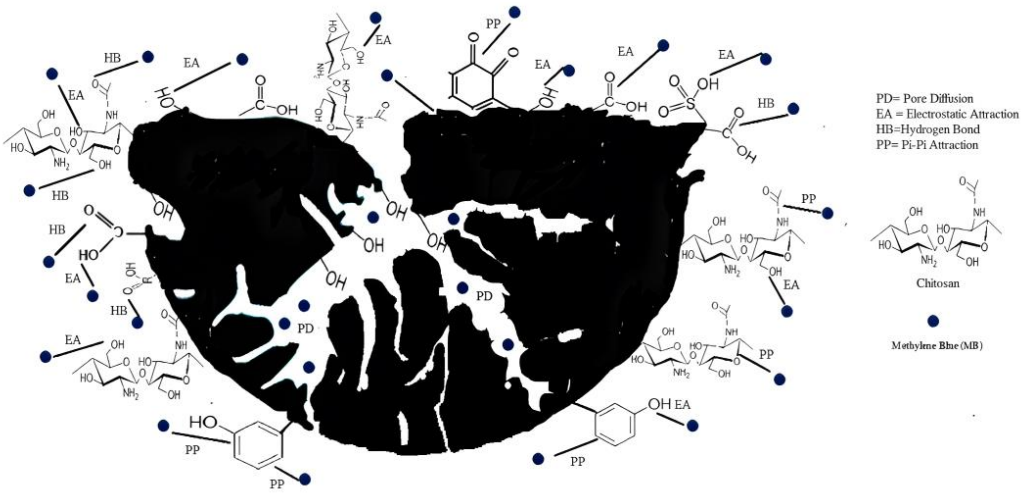


Figure 8. The proposed MB sorption mechanism of BC.

Table 6 summarizes different biochar and their modification approach for the sorption of MB. The banana pseudostem biochar was modified with phosphomolybdic acid ($H_3PMo_{12}O_{40}$), and an increase of ~67% in MB sorption capacity was achieved. The ferrous sulfate ($FeSO_4$) modified banana peel biochar showed a ~100% increase, whereas MnO_2-modified lignin biochar exhibited only ~6% increase. The zinc chloride ($ZnCl_2$), potassium hydroxide (KOH) and sulfuric acid (H_2SO_4) modified walnut shell biochar showed ~52, 10 and 0.5% increase, respectively. The BC prepared in this work showed ~127 increase compared to raw biochar. However, there are some sophisticated technologies that may increase the sorption capacities of raw biochar even more. Still, as an easy approach, the chitosan-modified biochar has immense potential to be the next-generation adsorption material.

Table 6. Different modified biochar and their characteristics.

Different Biochar	Experimental Conditions	Surface Area m^2/g	Pore Volume (cm^3/g)	Preferred Isotherm Model	Absorption Capacity mg/g	Absorption Mechanism	Reference
Banana pseudostem biochar	40 mL 50 mg/L MB solution, 1.25 g/L biochar, pH = 5.62, 20 °C	1.186	0.00780	Langmuir	87.28	Electrostatic interactions, and ion exchange	[132]
Phosphomolybdic acid ($H_3PMo_{12}O_{40}$) modified banana Pseudostem biochar	40 mL 50 mg/L MB solution, 1.25 g/L modified biochar, pH = 3.64, 45 °C	3.741	0.01234		146.23		
Banana peel biochar	20 mL 50 mg/L MB solution, pH 2.05–9.1, 20 °C, 12 h	N/A	N/A	Langmuir	429	N/A	[133]
Ferrous sulfate ($FeSO_4$) modified banana peel biochar	20 mL 50 mg/L MB solution, pH 2.05–9.1, 20 °C, 12 h	N/A	N/A		862		
Lychee seed biochar	500 mL MB solution, 10–100 mg/L raw/modified biochar, pH = 2–12, 2 h	138	0.068	Langmuir	N/A	π-π interactions	[134]
Potassium hydroxide (KOH) modified lychee seed biochar		154	0.051		124.5		
Lignin Biochar	5–100 mg/L MB solution, pH = 11, 2 h	48.136	0.029	Langmuir	234.65	N/A	[134]
Manganese dioxide (MnO_2) modified lignin biochar		349.946	0.447		248.96		
Sawdust ozone biochar	100 mg/L MB solution, 0.5–4 g/L raw/modified biochar, pH = 2–12	2.1516	0.0057151 m^3/g	Langmuir	200	Electrostatic interaction and hydrogen bonding	[135]
Sonicated sawdust ozone biochar		4.5740	0.015620 m^3/g		526		
Purified sawdust biochar	100 mg/L MB solution, 0.5–2.5 g/L raw/modified biochar, pH = 2–12	3.5890	0.012872 m^3/g		769		
Walnut shell biochar	50–300 mg/L MB solution, 0.5 g raw/modified biochar, pH = 2–11	194.77	0.1623	Freundlich	566.5	Physical absorption	[136]
Zinc chloride ($ZnCl_2$) modified Walnut shell biochar		534.40	0.3086		862.9		
KOH modified Walnut shell biochar		712.07	0.4082		625.2		
Sulfuric acid (H_2SO_4) modified Walnut shell biochar		114.34	0.0495		569.5		
Phosphoric acid (H_3PO_4) modified Walnut shell biochar		117.64	0.0926		563.6		
Corn stalk biochar	30 mL 50 mg/L MB solution, 50 0.5–4 g/L raw/modified biochar	24	0.021	Langmuir	45.58	Physical interaction, electrostatic interaction, hydrogen bonding and π-π interaction	[137]
KOH modified Corn stalk biochar		474	0.24		406.43		
H_3PO_4 modified Corn stalk biochar		3	0.0025		234.75		
M. oleifera seed biochar	10–70 mg/L MB solution = 3–9, 0.2 g/L raw/modified biochar, 1.5 h	0.96	N/A	Langmuir	78.92	Pore diffusion, electrostatic interaction, hydrogen bonding and π-π interaction	This work
Zinc oxide (ZnO) *M. oleifera* seed biochar		14.48			54.22		
Chitosan modified *M. oleifera* biochar		0.90			179.85		

5. Conclusions

The chitosan and ZnO-modified *M. oleifera* biochar-based binary composites were found to be abundant in different surface functional groups. The chitosan modification introduced larger chunks in the biochar surface. The biochar surface was fully amorphous, whereas a crystalline structure was found for other composites. The ZnO and chitosan modifications showed the highest and lowest surface area, respectively. The highest adsorption capacity was found for BC composite (179.8 mg dye/g), followed by biochar (78.9 mg dye/g), CZ (65.87 mg dye/g), ZnO (60.27 mg dye/g), BZ (54.22 mg dye/g) and chitosan (47.73 mg dye/g). The pseudo-2nd model better fits all the sorbents. Langmuir's model described the sorption process. The +ve/-ve surface/dye (electrostatic) interactions, hydrogen bonding (H-bond), and π-π interaction were critical sorption mechanisms of BC. The CCD-based RSM model predicted the BC/MB system well. The experimental data fit the quadratic (R^2 = 0.99) model. The model established for BC/MB system was found statistically justified with a non-significant lack of fit. The outcome of the chitosan-modified biochar compared to raw biochar was 75% enhanced performance which can be implemented for real textile wastewater treatment.

Supplementary Materials: The following supporting information can be downloaded at: https://www.mdpi.com/article/10.3390/su142114571/s1. Table S1: Independent parameters and their corresponding levels for percentage removal (% R) for BC. Table S2: The ANOVA analysis of variance quadratic model for removal of the dye.

Author Contributions: Conceptualization, H.R. and M.S.I.; formal analysis, H.R., M.T.A. and M.S.I.; writing—original draft and final paper preparation, H.R., M.S.I. and S.H.F.; writing—review and editing, H.R., M.T.A., M.S.I. and S.H.F.; supervision, M.S.I. and S.H.F.; project administration, M.S.I.; funding acquisition, M.S.I. All authors have read and agreed to the published version of the manuscript.

Funding: The research was funded by CASR (Committee for Advanced Studies & Research) of BUET (Bangladesh University of Engineering & Technology), Dhaka-1000, Bangladesh. Grant Number: 38-2020.

Data Availability Statement: The datasets generated during the current study are available from the corresponding author on reasonable request (Md. Shahinoor Islam, M.S.I.).

Acknowledgments: We would like to express our sincere gratitude for the support from the CASR (Committee for Advanced Studies & Research, BUET (Bangladesh University of Engineering & Technology), Dhaka, Bangladesh and Ehsanur Rahman for assisting in the lab work.

Conflicts of Interest: The authors declare no conflict of interest.

References

1. de Assis Filho, R.B.; Baptisttella, A.M.S.; de Araujo, C.M.B.; Fraga, T.J.M.; de Paiva, T.M.N.; de Abreu, C.A.M.; da Motta Sobrinho, M.A. Removal of textile dyes by benefited marine shells wastes: From circular economy to multi-phenomenological modeling. *J. Environ. Manag.* **2021**, *296*, 113222. [CrossRef] [PubMed]
2. Singha, K.; Pandit, P.; Maity, S.; Sharma, S.R. Chapter 11—Harmful environmental effects for textile chemical dyeing practice. In *Green Chemistry for Sustainable Textiles*; Ibrahim, N., Hussain, C.M., Eds.; Woodhead Publishing: Sawston, UK, 2021; pp. 153–164. [CrossRef]
3. Berradi, M.; Hsissou, R.; Khudhair, M.; Assouag, M.; Cherkaoui, O.; El Bachiri, A.; El Harfi, A. Textile finishing dyes and their impact on aquatic environs. *Heliyon* **2019**, *5*, e02711. [CrossRef] [PubMed]
4. Khan, S.; Malik, A. Environmental and Health Effects of Textile Industry Wastewater. In *Environmental Deterioration and Human Health: Natural and Anthropogenic Determinants*; Malik, A., Grohmann, E., Akhtar, R., Eds.; Springer: Dordrecht, The Netherlands, 2014; pp. 55–71. [CrossRef]
5. Sarwar, Z.; Tichonovas, M.; Krugly, E.; Masione, G.; Abromaitis, V.; Martuzevicius, D. Graphene oxide loaded fibrous matrixes of polyether block amide (PEBA) elastomer as an adsorbent for removal of cationic dye from wastewater. *J. Environ. Manag.* **2021**, *298*, 113466. [CrossRef] [PubMed]
6. Shuchi, S.B.; Suhan, M.B.K.; Humayun, S.B.; Haque, M.E.; Islam, M.S. Heat-activated potassium persulfate treatment of Sudan Black B dye: Degradation kinetic and thermodynamic studies. *J. Water Process Eng.* **2021**, *39*, 101690. [CrossRef]

7. Suhan, M.B.K.; Shuchi, S.B.; Anis, A.; Haque, Z.; Islam, M.S. Comparative degradation study of remazol black B dye using electro-coagulation and electro-Fenton process: Kinetics and cost analysis. *Environ. Nanotechnol. Monit. Manag.* **2020**, *14*, 100335. [CrossRef]
8. Akter, S.; Suhan, M.B.K.; Islam, M.S. Recent advances and perspective of electrocoagulation in the treatment of wastewater: A review. *Environ. Nanotechnol. Monit. Manag.* **2022**, *17*, 100643. [CrossRef]
9. Can-Güven, E. Advanced treatment of dye manufacturing wastewater by electrocoagulation and electro-Fenton processes: Effect on COD fractions, energy consumption, and sludge analysis. *J. Environ. Manag.* **2021**, *300*, 113784. [CrossRef]
10. Suhan, M.B.K.; Mahtab, S.M.T.; Aziz, W.; Akter, S.; Islam, M.S. Sudan black B dye degradation in aqueous solution by Fenton oxidation process: Kinetics and cost analysis. *Case Stud. Chem. Environ. Eng.* **2021**, *4*, 100126. [CrossRef]
11. Qian, W.; Huang, H.; Diao, Z.; Li, H.; Liu, H.; Ye, M.; Deng, Y.; Xu, Z. Advanced treatment of dye wastewater using a novel integrative Fenton-like/MnO_2-filled upward flow biological filter bed system equipped with modified ceramsite. *Environ. Res.* **2021**, *194*, 110641. [CrossRef]
12. Sadri Moghaddam, S.; Alavi Moghaddam, M.R.; Arami, M. Coagulation/flocculation process for dye removal using sludge from water treatment plant: Optimization through response surface methodology. *J. Hazard. Mater.* **2010**, *175*, 651–657. [CrossRef]
13. Akter, S.; Islam, M.S. Effect of additional Fe2+ salt on electrocoagulation process for the degradation of methyl orange dye: An optimization and kinetic study. *Heliyon* **2022**, *8*, e10176. [CrossRef] [PubMed]
14. Hassan, M.M.; Carr, C.M. A critical review on recent advancements of the removal of reactive dyes from dyehouse effluent by ion-exchange adsorbents. *Chemosphere* **2018**, *209*, 201–219. [CrossRef] [PubMed]
15. Karcher, S.; Kornmüller, A.; Jekel, M. Anion exchange resins for removal of reactive dyes from textile wastewaters. *Water Res.* **2002**, *36*, 4717–4724. [CrossRef]
16. Bhatia, D.; Sharma, N.R.; Singh, J.; Kanwar, R.S. Biological methods for textile dye removal from wastewater: A review. *Critical Rev. Environ. Sci. Technol.* **2017**, *47*, 1836–1876. [CrossRef]
17. Patel, Y.; Chhaya, U.; Rudakiya, D.M.; Joshi, S. Biological Decolorization and Degradation of Synthetic Dyes: A Green Step Toward Sustainable Environment. In *Microbial Rejuvenation of Polluted Environment: Volume 2*; Panpatte, D.G., Jhala, Y.K., Eds.; Springer: Singapore, 2021; pp. 77–110. [CrossRef]
18. Shoaib, M.; Ashar, A.; Bhutta, Z.A.; Muzammil, I.; Ali, M.; Kanwal, A. Chapter 15—Biological methods for degradation of textile dyes from textile effluent. In *Development in Wastewater Treatment Research and Processes*; Shah, M.P., Rodriguez-Couto, S., Kapoor, R.T., Eds.; Elsevier: Amsterdam, The Netherlands, 2022; pp. 329–353. [CrossRef]
19. Akter, S.; Islam, M.S.; Kabir, M.H.; Shaikh, M.A.A.; Gafur, M.A. UV/TiO_2 photodegradation of metronidazole, ciprofloxacin and sulfamethoxazole in aqueous solution: An optimization and kinetic study. *Arab. J. Chem.* **2022**, *15*, 103900. [CrossRef]
20. Al-Mamun, M.R.; Kader, S.; Islam, M.S. Solar-TiO_2 immobilized photocatalytic reactors performance assessment in the degradation of methyl orange dye in aqueous solution. *Environ. Nanotechnol. Monit. Manag.* **2021**, *16*, 100514. [CrossRef]
21. Al-Mamun, M.R.; Kader, S.; Islam, M.S.; Khan, M.Z.H. Photocatalytic activity improvement and application of UV-TiO_2 photocatalysis in textile wastewater treatment: A review. *J. Environ. Chem. Eng.* **2019**, *7*, 103248. [CrossRef]
22. Al-Mamun, M.R.; Karim, M.N.; Nitun, N.A.; Kader, S.; Islam, M.S.; Khan, M.Z.H. Photocatalytic performance assessment of GO and Ag co-synthesized TiO_2 nanocomposite for the removal of methyl orange dye under solar irradiation. *Environ. Technol. Innov.* **2021**, *22*, 101537. [CrossRef]
23. Hasan Khan Neon, M.; Islam, M.S. MoO_3 and Ag co-synthesized TiO_2 as a novel heterogeneous photocatalyst with enhanced visible-light-driven photocatalytic activity for methyl orange dye degradation. *Environ. Nanotechnol. Monit. Manag.* **2019**, *12*, 100244. [CrossRef]
24. Rashid Al-Mamun, M.; Hossain, K.T.; Mondal, S.; Afroza Khatun, M.; Shahinoor Islam, M.; Zaved Hossain Khan, D.M. Synthesis, characterization, and photocatalytic performance of methyl orange in aqueous TiO_2 suspension under UV and solar light irradiation. *S. Afr. J. Chem. Eng.* **2022**, *40*, 113–125. [CrossRef]
25. Rashid Al-Mamun, M.; Shofikul Islam, M.; Rasel Hossain, M.; Kader, S.; Shahinoor Islam, M.; Zaved Hossain Khan, M. A novel and highly efficient Ag and GO co-synthesized ZnO nano photocatalyst for methylene blue dye degradation under UV irradiation. *Environ. Nanotechnol. Monit. Manag.* **2021**, *16*, 100495. [CrossRef]
26. Tünay, O.; Kabdasli, I.; Eremektar, G.; Orhon, D. Color removal from textile wastewaters. *Water Sci. Technol.* **1996**, *34*, 9–16. [CrossRef]
27. Wang, L.K.; Vaccari, D.A.; Li, Y.; Shammas, N.K. Chemical Precipitation. In *Physicochemical Treatment Processes*; Wang, L.K., Hung, Y.-T., Shammas, N.K., Eds.; Humana Press: Totowa, NJ, USA, 2005; pp. 141–197. [CrossRef]
28. Islam, M.S.; Kwak, J.-H.; Nzediegwu, C.; Wang, S.; Palansuriya, K.; Kwon, E.E.; Naeth, M.A.; El-Din, M.G.; Ok, Y.S.; Chang, S.X. Biochar heavy metal removal in aqueous solution depends on feedstock type and pyrolysis purging gas. *Environ. Pollut.* **2021**, *281*, 117094. [CrossRef] [PubMed]
29. Islam, M.S.; McPhedran, K.N.; Messele, S.A.; Liu, Y.; Gamal El-Din, M. Isotherm and kinetic studies on adsorption of oil sands process-affected water organic compounds using granular activated carbon. *Chemosphere* **2018**, *202*, 716–725. [CrossRef]
30. Islam, M.S.; Roy, H.; Afrose, S. Phosphoric acid surface modified Moringa oleifera leaves biochar for the sequestration of methyl orange from aqueous solution: Characterizations, isotherm, and kinetics analysis. *Remediat. J.* **2022**, *32*, 281–298. [CrossRef]
31. Jahan, N.; Roy, H.; Reaz, A.H.; Arshi, S.; Rahman, E.; Firoz, S.H.; Islam, M.S. A comparative study on sorption behavior of graphene oxide and reduced graphene oxide towards methylene blue. *Case Stud. Chem. Environ. Eng.* **2022**, *6*, 100239. [CrossRef]

32. Kwak, J.-H.; Islam, M.S.; Wang, S.; Messele, S.A.; Naeth, M.A.; El-Din, M.G.; Chang, S.X. Biochar properties and lead(II) adsorption capacity depend on feedstock type, pyrolysis temperature, and steam activation. *Chemosphere* **2019**, *231*, 393–404. [CrossRef]
33. Roy, H.; Prantika, T.R.; Riyad, M.H.; Paul, S.; Islam, M.S. Synthesis, characterizations, and RSM analysis of Citrus macroptera peel derived biochar for textile dye treatment. *S. Afr. J. Chem. Eng.* **2022**, *41*, 129–139. [CrossRef]
34. Roy, H.; Shahinoor Islam, M.; Tanvir Arifin, M.; Firoz, S.H. Chitosan-ZnO decorated Moringa oleifera seed biochar for sequestration of methylene blue: Isotherms, kinetics, and response surface analysis. *Environ. Nanotechnol. Monit. Manag.* **2022**, *18*, 100752. [CrossRef]
35. Wang, S.; Ai, S.; Nzediegwu, C.; Kwak, J.-H.; Islam, M.S.; Li, Y.; Chang, S.X. Carboxyl and hydroxyl groups enhance ammonium adsorption capacity of iron (III) chloride and hydrochloric acid modified biochars. *Bioresour. Technol.* **2020**, *309*, 123390. [CrossRef]
36. Samsami, S.; Mohamadizaniani, M.; Sarrafzadeh, M.-H.; Rene, E.R.; Firoozbahr, M. Recent advances in the treatment of dye-containing wastewater from textile industries: Overview and perspectives. *Process Saf. Environ. Prot.* **2020**, *143*, 138–163. [CrossRef]
37. Gupta, V.K.; Suhas. Application of low-cost adsorbents for dye removal—A review. *J. Environ. Manag.* **2009**, *90*, 2313–2342. [CrossRef] [PubMed]
38. Hynes, N.R.J.; Kumar, J.S.; Kamyab, H.; Sujana, J.A.J.; Al-Khashman, O.A.; Kuslu, Y.; Ene, A.; Suresh Kumar, B. Modern enabling techniques and adsorbents based dye removal with sustainability concerns in textile industrial sector -A comprehensive review. *J. Clean. Prod.* **2020**, *272*, 122636. [CrossRef]
39. Morais da Silva, P.M.; Camparotto, N.G.; Grego Lira, K.T.; Franco Picone, C.S.; Prediger, P. Adsorptive removal of basic dye onto sustainable chitosan beads: Equilibrium, kinetics, stability, continuous-mode adsorption and mechanism. *Sustain. Chem. Pharm.* **2020**, *18*, 100318. [CrossRef]
40. Dutta, S.; Gupta, B.; Srivastava, S.K.; Gupta, A.K. Recent advances on the removal of dyes from wastewater using various adsorbents: A critical review. *Mater. Adv.* **2021**, *2*, 4497–4531. [CrossRef]
41. Saxena, M.; Sharma, N.; Saxena, R. Highly efficient and rapid removal of a toxic dye: Adsorption kinetics, isotherm, and mechanism studies on functionalized multiwalled carbon nanotubes. *Surf. Interfaces* **2020**, *21*, 100639. [CrossRef]
42. Ahmed, M.N.; Ram, R.N. Removal of basic dye from waste-water using silica as adsorbent. *Environ. Pollut.* **1992**, *77*, 79–86. [CrossRef]
43. Banerjee, S.; Dubey, S.; Gautam, R.K.; Chattopadhyaya, M.C.; Sharma, Y.C. Adsorption characteristics of alumina nanoparticles for the removal of hazardous dye, Orange G from aqueous solutions. *Arab. J. Chem.* **2019**, *12*, 5339–5354. [CrossRef]
44. Wang, C.; Li, J.; Wang, L.; Sun, X.; Huang, J. Adsorption of Dye from Wastewater by Zeolites Synthesized from Fly Ash: Kinetic and Equilibrium Studies. *Chin. J. Chem. Eng.* **2009**, *17*, 513–521. [CrossRef]
45. Tahir, S.S.; Rauf, N. Removal of a cationic dye from aqueous solutions by adsorption onto bentonite clay. *Chemosphere* **2006**, *63*, 1842–1848. [CrossRef]
46. Bradder, P.; Ling, S.K.; Wang, S.; Liu, S. Dye Adsorption on Layered Graphite Oxide. *J. Chem. Eng. Data* **2011**, *56*, 138–141. [CrossRef]
47. Yang, S.-T.; Chen, S.; Chang, Y.; Cao, A.; Liu, Y.; Wang, H. Removal of methylene blue from aqueous solution by graphene oxide. *J. Colloid Interface Sci.* **2011**, *359*, 24–29. [CrossRef] [PubMed]
48. Gómez, V.; Larrechi, M.S.; Callao, M.P. Kinetic and adsorption study of acid dye removal using activated carbon. *Chemosphere* **2007**, *69*, 1151–1158. [CrossRef] [PubMed]
49. Herrera-González, A.M.; Caldera-Villalobos, M.; Peláez-Cid, A.-A. Adsorption of textile dyes using an activated carbon and crosslinked polyvinyl phosphonic acid composite. *J. Environ. Manag.* **2019**, *234*, 237–244. [CrossRef]
50. Nautiyal, P.; Subramanian, K.A.; Dastidar, M.G. Adsorptive removal of dye using biochar derived from residual algae after in-situ transesterification: Alternate use of waste of biodiesel industry. *J. Environ. Manag.* **2016**, *182*, 187–197. [CrossRef]
51. Qiu, Y.; Zheng, Z.; Zhou, Z.; Sheng, G.D. Effectiveness and mechanisms of dye adsorption on a straw-based biochar. *Bioresour. Technol.* **2009**, *100*, 5348–5351. [CrossRef]
52. Sackey, E.A.; Song, Y.; Yu, Y.; Zhuang, H. Biochars derived from bamboo and rice straw for sorption of basic red dyes. *PLoS ONE* **2021**, *16*, e0254637. [CrossRef]
53. Sumalinog, D.A.G.; Capareda, S.C.; de Luna, M.D.G. Evaluation of the effectiveness and mechanisms of acetaminophen and methylene blue dye adsorption on activated biochar derived from municipal solid wastes. *J. Environ. Manag.* **2018**, *210*, 255–262. [CrossRef]
54. Ikram, R.; Jan, B.M.; Ahmad, W. Advances in synthesis of graphene derivatives using industrial wastes precursors; prospects and challenges. *J. Mater. Res. Technol.* **2020**, *9*, 15924–15951. [CrossRef]
55. Katheresan, V.; Kansedo, J.; Lau, S.Y. Efficiency of various recent wastewater dye removal methods: A review. *J. Environ. Chem. Eng.* **2018**, *6*, 4676–4697. [CrossRef]
56. Smith, A.T.; LaChance, A.M.; Zeng, S.; Liu, B.; Sun, L. Synthesis, properties, and applications of graphene oxide/reduced graphene oxide and their nanocomposites. *Nano Mater. Sci.* **2019**, *1*, 31–47. [CrossRef]
57. Pan, X.; Gu, Z.; Chen, W.; Li, Q. Preparation of biochar and biochar composites and their application in a Fenton-like process for wastewater decontamination: A review. *Sci. Total Environ.* **2021**, *754*, 142104. [CrossRef] [PubMed]

58. Patawat, C.; Silakate, K.; Chuan-Udom, S.; Supanchaiyamat, N.; Hunt, A.J.; Ngernyen, Y. Preparation of activated carbon from Dipterocarpus alatus fruit and its application for methylene blue adsorption. *RSC Adv.* **2020**, *10*, 21082–21091. [CrossRef] [PubMed]
59. Yaashikaa, P.R.; Kumar, P.S.; Varjani, S.; Saravanan, A. A critical review on the biochar production techniques, characterization, stability and applications for circular bioeconomy. *Biotechnol. Rep.* **2020**, *28*, e00570. [CrossRef]
60. Yakout, S.M.; Sharaf El-Deen, G. Characterization of activated carbon prepared by phosphoric acid activation of olive stones. *Arab. J. Chem.* **2016**, *9*, S1155–S1162. [CrossRef]
61. Oliveira, F.R.; Patel, A.K.; Jaisi, D.P.; Adhikari, S.; Lu, H.; Khanal, S.K. Environmental application of biochar: Current status and perspectives. *Bioresour. Technol.* **2017**, *246*, 110–122. [CrossRef]
62. Wang, S.; Kwak, J.-H.; Islam, M.S.; Naeth, M.A.; Gamal El-Din, M.; Chang, S.X. Biochar surface complexation and Ni(II), Cu(II), and Cd(II) adsorption in aqueous solutions depend on feedstock type. *Sci. Total Environ.* **2020**, *712*, 136538. [CrossRef]
63. Rangabhashiyam, S.; Balasubramanian, P. The potential of lignocellulosic biomass precursors for biochar production: Performance, mechanism and wastewater application—A review. *Ind. Crops Prod.* **2019**, *128*, 405–423. [CrossRef]
64. Zhao, T.; Ma, X.; Cai, H.; Ma, Z.; Liang, H. Study on the Adsorption of $CuFe_2O_4$-Loaded Corncob Biochar for Pb(II). *Molecules* **2020**, *25*, 3456. [CrossRef]
65. Wang, L.; Wang, Y.; Ma, F.; Tankpa, V.; Bai, S.; Guo, X.; Wang, X. Mechanisms and reutilization of modified biochar used for removal of heavy metals from wastewater: A review. *Sci. Total Environ.* **2019**, *668*, 1298–1309. [CrossRef]
66. Gao, N.; Du, W.; Zhang, M.; Ling, G.; Zhang, P. Chitosan-modified biochar: Preparation, modifications, mechanisms and applications. *Int. J. Biol. Macromol.* **2022**, *209*, 31–49. [CrossRef] [PubMed]
67. Vigneshwaran, S.; Sirajudheen, P.; Nikitha, M.; Ramkumar, K.; Meenakshi, S. Facile synthesis of sulfur-doped chitosan/biochar derived from tapioca peel for the removal of organic dyes: Isotherm, kinetics and mechanisms. *J. Mol. Liq.* **2021**, *326*, 115303. [CrossRef]
68. Wang, F.; Li, L.; Iqbal, J.; Yang, Z.; Du, Y. Preparation of magnetic chitosan corn straw biochar and its application in adsorption of amaranth dye in aqueous solution. *Int. J. Biol. Macromol.* **2022**, *199*, 234–242. [CrossRef] [PubMed]
69. Chen, M.; Bao, C.; Hu, D.; Jin, X.; Huang, Q. Facile and low-cost fabrication of ZnO/biochar nanocomposites from jute fibers for efficient and stable photodegradation of methylene blue dye. *J. Anal. Appl. Pyrolysis* **2019**, *139*, 319–332. [CrossRef]
70. Leichtweis, J.; Silvestri, S.; Carissimi, E. New composite of pecan nutshells biochar-ZnO for sequential removal of acid red 97 by adsorption and photocatalysis. *Biomass Bioenergy* **2020**, *140*, 105648. [CrossRef]
71. Mehmood, S.; Ahmed, W.; Ikram, M.; Imtiaz, M.; Mahmood, S.; Tu, S.; Chen, D. Chitosan Modified Biochar Increases Soybean (*Glycine max* L.) Resistance to Salt-Stress by Augmenting Root Morphology, Antioxidant Defense Mechanisms and the Expression of Stress-Responsive Genes. *Plants* **2020**, *9*, 1173. [CrossRef]
72. Cruz, G.J.F.; Mondal, D.; Rimaycuna, J.; Soukup, K.; Gómez, M.M.; Solis, J.L.; Lang, J. Agrowaste derived biochars impregnated with ZnO for removal of arsenic and lead in water. *J. Environ. Chem. Eng.* **2020**, *8*, 103800. [CrossRef]
73. Arafat, A.; Samad, S.; Huq, D.; Moniruzzaman, M.; Masum, M. Textile Dye Removal from Wastewater Effluents Using Chitosan-ZnO Nanocomposite. *OMICS Int. J. Text. Sci. Eng.* **2015**, *5*, 1000200. [CrossRef]
74. Nnaji, C.C.; Agim, A.E.; Mama, C.N.; Emenike, P.C.; Ogarekpe, N.M. Equilibrium and thermodynamic investigation of biosorption of nickel from water by activated carbon made from palm kernel chaff. *Sci. Rep.* **2021**, *11*, 7808. [CrossRef]
75. Ghosh, I.; Kar, S.; Chatterjee, T.; Bar, N.; Das, S.K. Removal of methylene blue from aqueous solution using Lathyrus sativus husk: Adsorption study, MPR and ANN modelling. *Process Saf. Environ. Prot.* **2021**, *149*, 345–361. [CrossRef]
76. Revellame, E.D.; Fortela, D.L.; Sharp, W.; Hernandez, R.; Zappi, M.E. Adsorption kinetic modeling using pseudo-first order and pseudo-second order rate laws: A review. *Clean. Eng. Technol.* **2020**, *1*, 100032. [CrossRef]
77. Chahinez, H.-O.; Abdelkader, O.; Leila, Y.; Tran, H.N. One-stage preparation of palm petiole-derived biochar: Characterization and application for adsorption of crystal violet dye in water. *Environ. Technol. Innov.* **2020**, *19*, 100872. [CrossRef]
78. Li, L.; Chen, Q.; Zhao, C.; Guo, B.; Xu, X.; Liu, T.; Zhao, L. A novel chitosan modified magnesium impregnated corn straw biochar for ammonium and phosphate removal from simulated livestock wastewater. *Environ. Technol. Innov.* **2022**, *26*, 102519. [CrossRef]
79. Wu, M.; Feng, Q.; Sun, X.; Wang, H.; Gielen, G.; Wu, W. Rice (*Oryza sativa* L.) plantation affects the stability of biochar in paddy soil. *Sci. Rep.* **2015**, *5*, 10001. [CrossRef] [PubMed]
80. Al-Ghouti, M.A.; Khraisheh, M.A.M.; Allen, S.J.; Ahmad, M.N. The removal of dyes from textile wastewater: A study of the physical characteristics and adsorption mechanisms of diatomaceous earth. *J. Environ. Manag.* **2003**, *69*, 229–238. [CrossRef]
81. Pradeep Sekhar, C.; Kalidhasan, S.; Rajesh, V.; Rajesh, N. Bio-polymer adsorbent for the removal of malachite green from aqueous solution. *Chemosphere* **2009**, *77*, 842–847. [CrossRef]
82. Jing, H.; Ji, L.; Wang, Z.; Guo, J.; Lu, S.; Sun, J.; Cai, L.; Wang, Y. Synthesis of ZnO Nanoparticles Loaded on Biochar Derived from Spartina alterniflora with Superior Photocatalytic Degradation Performance. *Nanomaterials* **2021**, *11*, 2479. [CrossRef]
83. Beil, S.; Schamberger, A.; Naumann, W.; Machill, S.; van Pée, K.-H. Determination of the degree of N-acetylation (DA) of chitin and chitosan in the presence of water by first derivative ATR FTIR spectroscopy. *Carbohydr. Polym.* **2012**, *87*, 117–122. [CrossRef]
84. Pandiyarajan, T.; Karthikeyan, B. Optical properties of annealing induced post growth ZnO:$ZnFe_2O_4$ nanocomposites. *Spectrochim. Acta Part A Mol. Biomol. Spectrosc.* **2013**, *106*, 247–252. [CrossRef]
85. Janu, R.; Mrlik, V.; Ribitsch, D.; Hofman, J.; Sedláček, P.; Bielská, L.; Soja, G. Biochar surface functional groups as affected by biomass feedstock, biochar composition and pyrolysis temperature. *Carbon Resour. Convers.* **2021**, *4*, 36–46. [CrossRef]

86. Acharyulu, S.R.; Gomathi, T.; Sudha, P.N. Physico-chemical characterization of cross linked chitosan-polyacrylonitrile polymer blends. *Der Pharm. Lett.* **2013**, *5*, 354–363.
87. Shaaban, A.; Se, S.-M.; Mitan, N.M.M.; Dimin, M.F. Characterization of Biochar Derived from Rubber Wood Sawdust through Slow Pyrolysis on Surface Porosities and Functional Groups. *Procedia Eng.* **2013**, *68*, 365–371. [CrossRef]
88. Nartey, O.D.; Zhao, B. Biochar Preparation, Characterization, and Adsorptive Capacity and Its Effect on Bioavailability of Contaminants: An Overview. *Adv. Mater. Sci. Eng.* **2014**, *2014*, 715398. [CrossRef]
89. Abd-Elhamid, A.I.; Emran, M.; El-Sadek, M.H.; El-Shanshory, A.A.; Soliman, H.M.A.; Akl, M.A.; Rashad, M. Enhanced removal of cationic dye by eco-friendly activated biochar derived from rice straw. *Appl. Water Sci.* **2020**, *10*, 45. [CrossRef]
90. Bagheri, A.; Abu-Danso, E.; Iqbal, J.; Bhatnagar, A. Modified biochar from Moringa seed powder for the removal of diclofenac from aqueous solution. *Environ. Sci. Pollut. Res.* **2020**, *27*, 7318–7327. [CrossRef] [PubMed]
91. Hammo, M.M.; Akar, T.; Sayın, F.; Celik, S.; Tunali Akar, S. Efficacy of green waste-derived biochar for lead removal from aqueous systems: Characterization, equilibrium, kinetic and application. *J. Environ. Manag.* **2021**, *289*, 112490. [CrossRef] [PubMed]
92. Suman, S.; Panwar, D.S.; Gautam, S. Surface morphology properties of biochars obtained from different biomass waste. *Energy Sources Part A Recovery Util. Environ. Eff.* **2017**, *39*, 1007–1012. [CrossRef]
93. Eddya, M.; Tbib, B.; El-Hami, K. A comparison of chitosan properties after extraction from shrimp shells by diluted and concentrated acids. *Heliyon* **2020**, *6*, e03486. [CrossRef]
94. Geetha, M.S.; Nagabhushana, H.; Shivananjaiah, H.N. Green mediated synthesis and characterization of ZnO nanoparticles using Euphorbia Jatropa latex as reducing agent. *J. Sci. Adv. Mater. Devices* **2016**, *1*, 301–310. [CrossRef]
95. Zhou, Y.; Gao, B.; Zimmerman, A.R.; Fang, J.; Sun, Y.; Cao, X. Sorption of heavy metals on chitosan-modified biochars and its biological effects. *Chem. Eng. J.* **2013**, *231*, 512–518. [CrossRef]
96. Banerjee, S.; Chattopadhyaya, M.C. Adsorption characteristics for the removal of a toxic dye, tartrazine from aqueous solutions by a low cost agricultural by-product. *Arab. J. Chem.* **2017**, *10*, S1629–S1638. [CrossRef]
97. Tsamo, C.; Assabe, M.; Argue, J.; Ihimbru, S.O. Discoloration of methylene blue and slaughter house wastewater using maize cob biochar produced using a constructed burning chamber: A comparative study. *Sci. Afr.* **2019**, *3*, e00078. [CrossRef]
98. Tang, R.; Dai, C.; Li, C.; Liu, W.; Gao, S.; Wang, C. Removal of Methylene Blue from Aqueous Solution Using Agricultural Residue Walnut Shell: Equilibrium, Kinetic, and Thermodynamic Studies. *J. Chem.* **2017**, *2017*, 8404965. [CrossRef]
99. Zhu, H.-Y.; Jiang, R.; Xiao, L. Adsorption of an anionic azo dye by chitosan/kaolin/γ-Fe_2O_3 composites. *Appl. Clay Sci.* **2010**, *48*, 522–526. [CrossRef]
100. Amode, J.O.; Santos, J.H.; Mirza, A.H.; Mei, C.C. Adsorption of methylene blue from aqueous solution using untreated and treated (*Metroxylon* spp.) waste adsorbent: Equilibrium and kinetics studies. *Int. J. Ind. Chemistry* **2016**, *7*, 333–345. [CrossRef]
101. Keerthanan, S.; Rajapaksha, S.M.; Trakal, L.; Vithanage, M. Caffeine removal by Gliricidia sepium biochar: Influence of pyrolysis temperature and physicochemical properties. *Environ. Res.* **2020**, *189*, 109865. [CrossRef]
102. Jin, Q.; Li, Y.; Yang, D.; Cui, J. Chitosan-derived three-dimensional porous carbon for fast removal of methylene blue from wastewater. *RSC Adv.* **2018**, *8*, 1255–1264. [CrossRef]
103. Zubair, M.; Aziz, H.A.; Ihsanullah, I.; Ahmad, M.A.; Al-Harthi, M.A. Enhanced removal of Eriochrome Black T from water using biochar/layered double hydroxide/chitosan hybrid composite: Performance evaluation and optimization using BBD-RSM approach. *Environ.Research* **2022**, *209*, 112861. [CrossRef]
104. Roy, H.; Shakil, R.; Tarek, Y.A.; Firoz, S.H. Study of the Removal of Basic Blue-41 from Simulated Wastewater By Activated Carbon Prepared from Discarded Jute Fibre. *ECS Trans.* **2022**, *107*, 8407–8420. [CrossRef]
105. Hassan, H.; Salama, A.; El-ziaty, A.K.; El-Sakhawy, M. New chitosan/silica/zinc oxide nanocomposite as adsorbent for dye removal. *Int. J. Biol. Macromol.* **2019**, *131*, 520–526. [CrossRef]
106. Aichour, A.; Zaghouane-Boudiaf, H.; Djafer Khodja, H. Highly removal of anionic dye from aqueous medium using a promising biochar derived from date palm petioles: Characterization, adsorption properties and reuse studies. *Arab. J. Chem.* **2022**, *15*, 103542. [CrossRef]
107. Song, C.; Chen, K.; Chen, M.; Jin, X.; Liu, G.; Du, X.; Chen, D.; Huang, Q. Sequential combined adsorption and solid-phase photocatalysis to remove aqueous organic pollutants by H_3PO_4-modified TiO_2 nanoparticles anchored on biochar. *J. Water Process Eng.* **2022**, *45*, 102467. [CrossRef]
108. Sultan, M.; Mansor, E.S.; Nagieb, Z.A.; Elsayed, H. Fabrication of highly efficient nano-composite films based on ZnO-g-C_3N_4 @ PAA-g-(HEC/PVA)-Fe^{3+} for removal of methylene blue dye from water. *J. Water Process Eng.* **2021**, *42*, 102184. [CrossRef]
109. Muinde, V.M.; Onyari, J.M.; Wamalwa, B.; Wabomba, J.N. Adsorption of malachite green dye from aqueous solutions using mesoporous chitosan–zinc oxide composite material. *Environ. Chem. Ecotoxicol.* **2020**, *2*, 115–125. [CrossRef]
110. Al-Ghouti, M.A.; Al-Absi, R.S. Mechanistic understanding of the adsorption and thermodynamic aspects of cationic methylene blue dye onto cellulosic olive stones biomass from wastewater. *Sci. Rep.* **2020**, *10*, 15928. [CrossRef]
111. Bayomie, O.S.; Kandeel, H.; Shoeib, T.; Yang, H.; Youssef, N.; El-Sayed, M.M.H. Novel approach for effective removal of methylene blue dye from water using fava bean peel waste. *Sci. Rep.* **2020**, *10*, 7824. [CrossRef]
112. Wang, W.; Lu, T.; Chen, Y.; Tian, G.; Sharma, V.K.; Zhu, Y.; Zong, L.; Wang, A. Mesoporous silicate/carbon composites derived from dye-loaded palygorskite clay waste for efficient removal of organic contaminants. *Sci. Total Environ.* **2019**, *696*, 133955. [CrossRef]

113. Hussain, I.; Li, Y.; Qi, J.; Li, J.; Wang, L. Nitrogen-enriched carbon sheet for Methyl blue dye adsorption. *J. Environ. Manag.* **2018**, *215*, 123–131. [CrossRef]
114. Jasper, E.E.; Ajibola, V.O.; Onwuka, J.C. Nonlinear regression analysis of the sorption of crystal violet and methylene blue from aqueous solutions onto an agro-waste derived activated carbon. *Appl. Water Sci.* **2020**, *10*, 132. [CrossRef]
115. Tseng, R.-L.; Wu, F.-C.; Juang, R.-S. Liquid-phase adsorption of dyes and phenols using pinewood-based activated carbons. *Carbon* **2003**, *41*, 487–495. [CrossRef]
116. Ayawei, N.; Ebelegi, A.N.; Wankasi, D. Modelling and Interpretation of Adsorption Isotherms. *J. Chem.* **2017**, *2017*, 3039817. [CrossRef]
117. Takkar, S.; Tyagi, B.; Kumar, N.; Kumari, T.; Iqbal, K.; Varma, A.; Thakur, I.S.; Mishra, A. Biodegradation of methyl red dye by a novel actinobacterium Zhihengliuella sp. ISTPL4: Kinetic studies, isotherm and biodegradation pathway. *Environ. Technol. Innov.* **2022**, *26*, 102348. [CrossRef]
118. Nguyen, B.T.; Dinh, G.D.; Dong, H.P.; Le, L.B. Sodium adsorption isotherm and characterization of biochars produced from various agricultural biomass wastes. *J. Clean. Prod.* **2022**, *346*, 131250. [CrossRef]
119. Singh, M.; Ahsan, M.; Pandey, V.; Singh, A.; Mishra, D.; Tiwari, N.; Singh, P.; Karak, T.; Khare, P. Comparative assessment for removal of anionic dye from water by different waste-derived biochar vis a vis reusability of generated sludge. *Biochar* **2022**, *4*, 13. [CrossRef]
120. Yang, X.; Wan, Y.; Zheng, Y.; He, F.; Yu, Z.; Huang, J.; Wang, H.; Ok, Y.S.; Jiang, Y.; Gao, B. Surface functional groups of carbon-based adsorbents and their roles in the removal of heavy metals from aqueous solutions: A critical review. *Chem. Eng. J.* **2019**, *366*, 608–621. [CrossRef] [PubMed]
121. Shaikh, W.A.; Kumar, A.; Chakraborty, S.; Islam, R.U.; Bhattacharya, T.; Biswas, J.K. Biochar-based nanocomposite from waste tea leaf for toxic dye removal: From facile fabrication to functional fitness. *Chemosphere* **2022**, *291*, 132788. [CrossRef]
122. Tran, H.N.; Wang, Y.-F.; You, S.-J.; Chao, H.-P. Insights into the mechanism of cationic dye adsorption on activated charcoal: The importance of π–π interactions. *Process Saf. Environ. Prot.* **2017**, *107*, 168–180. [CrossRef]
123. Ahmad, M.; Ahmad, M.M.; Hamid, R.; Abdin, M.; Javed, S. Use of response surface methodology to study the effect of media composition on aflatoxin production by Aspergillus flavus. *Mycotoxin Res.* **2013**, *29*, 39–45. [CrossRef]
124. Abdulhameed, A.S.; Jawad, A.H.; Mohammad, A.-T. Synthesis of chitosan-ethylene glycol diglycidyl ether/TiO_2 nanoparticles for adsorption of reactive orange 16 dye using a response surface methodology approach. *Bioresour. Technol.* **2019**, *293*, 122071. [CrossRef]
125. Karri, R.R.; Tanzifi, M.; Tavakkoli Yaraki, M.; Sahu, J.N. Optimization and modeling of methyl orange adsorption onto polyaniline nano-adsorbent through response surface methodology and differential evolution embedded neural network. *J. Environ. Manag.* **2018**, *223*, 517–529. [CrossRef]
126. Cui, L.; Fan, Q.; Sun, J.; Quan, G.; Yan, J.; Hina, K.; Wang, H.; Zhang, Z.; Hussain, Q. Changes in surface characteristics and adsorption properties of 2,4,6-trichlorophenol following Fenton-like aging of biochar. *Sci. Rep.* **2021**, *11*, 4293. [CrossRef] [PubMed]
127. Oyekanmi, A.A.; Ahmad, A.; Mohd Setapar, S.H.; Alshammari, M.B.; Jawaid, M.; Hanafiah, M.M.; Abdul Khalil, H.P.S.; Vaseashta, A. Sustainable Durio zibethinus-Derived Biosorbents for Congo Red Removal from Aqueous Solution: Statistical Optimization, Isotherms and Mechanism Studies. *Sustainability* **2021**, *13*, 13264. [CrossRef]
128. Kasozi, G.N.; Zimmerman, A.R.; Nkedi-Kizza, P.; Gao, B. Catechol and Humic Acid Sorption onto a Range of Laboratory-Produced Black Carbons (Biochars). *Environ. Sci. Technol.* **2010**, *44*, 6189–6195. [CrossRef] [PubMed]
129. Suleman, M.; Zafar, M.; Ahmed, A.; Rashid, M.U.; Hussain, S.; Razzaq, A.; Mohidem, N.A.; Fazal, T.; Haider, B.; Park, Y.-K. Castor Leaves-Based Biochar for Adsorption of Safranin from Textile Wastewater. *Sustainability* **2021**, *13*, 6926. [CrossRef]
130. Almarri, M.; Ma, X.; Song, C. Role of Surface Oxygen-Containing Functional Groups in Liquid-Phase Adsorption of Nitrogen Compounds on Carbon-Based Adsorbents. *Energy Fuels* **2009**, *23*, 3940–3947. [CrossRef]
131. Zhang, X.; Wang, H.; He, L.; Lu, K.; Sarmah, A.; Li, J.; Bolan, N.S.; Pei, J.; Huang, H. Using biochar for remediation of soils contaminated with heavy metals and organic pollutants. *Environ. Sci. Pollut. Res.* **2013**, *20*, 8472–8483. [CrossRef]
132. Liu, S.; Li, J.; Xu, S.; Wang, M.; Zhang, Y.; Xue, X. A modified method for enhancing adsorption capability of banana pseudostem biochar towards methylene blue at low temperature. *Bioresour. Technol.* **2019**, *282*, 48–55. [CrossRef]
133. Zhang, P.; O'Connor, D.; Wang, Y.; Jiang, L.; Xia, T.; Wang, L.; Tsang, D.C.W.; Ok, Y.S.; Hou, D. A green biochar/iron oxide composite for methylene blue removal. *J. Hazard. Mater.* **2020**, *384*, 121286. [CrossRef]
134. Sahu, S.; Pahi, S.; Tripathy, S.; Singh, S.K.; Behera, A.; Sahu, U.K.; Patel, R.K. Adsorption of methylene blue on chemically modified lychee seed biochar: Dynamic, equilibrium, and thermodynamic study. *J. Mol. Liq.* **2020**, *315*, 113743. [CrossRef]
135. Eldeeb, T.M.; Aigbe, U.O.; Ukhurebor, K.E.; Onyancha, R.B.; El-Nemr, M.A.; Hassaan, M.A.; Ragab, S.; Osibote, O.A.; El Nemr, A. Adsorption of methylene blue (MB) dye on ozone, purified and sonicated sawdust biochars. *Biomass Convers. Biorefinery* **2022**. [CrossRef]
136. Liu, C.; Wang, W.; Wu, R.; Liu, Y.; Lin, X.; Kan, H.; Zheng, Y. Preparation of Acid- and Alkali-Modified Biochar for Removal of Methylene Blue Pigment. *ACS Omega* **2020**, *5*, 30906–30922. [CrossRef] [PubMed]
137. Liu, L.; Li, Y.; Fan, S. Preparation of KOH and H_3PO_4 Modified Biochar and Its Application in Methylene Blue Removal from Aqueous Solution. *Processes* **2019**, *7*, 891. [CrossRef]